NONINVASIVE ASSESSMENT OF TUMOR HYPOXIA USING OXYGEN SENSITIVE MRI IN PROSTATE TUMOR MODELS

by

RASHMI REDDY PABHATHI REDDY

Presented to the Faculty of the Graduate School of

The University of Texas at Arlington in Partial Fulfillment

of the Requirements

for the Degree of

MASTER OF SCIENCE IN BIOENGINEERING

THE UNIVERSITY OF TEXAS AT ARLINGTON

May 2013

ACKNOWLEDGEMENTS

There have been many people who contributed directly or indirectly to my research work. I like to express my gratitude and deepest appreciation to all of them, named or unnamed.

My deep gratitude goes to my mentor, Dr. Ralph P. Mason, for introducing me to MRI and the cancer research field. I deeply appreciate his constant encouragement, support in my study and research. Deepest gratitude is also due to the members of the supervisory committee, Dr. Khosrow Behbehani, Dr. Hanli Liu for their valuable suggestions and guidance.

I am grateful to every member of the Laboratory of Prognostic Radiology, especially Dr. Srinivas Chiguru, Dr. Rami Hallac, Dr. Zhongwei Zhang, Dr. Heling Zhou and staff members of the Radiology department who rendered their help during the period of my project work.

Last but not least, I would like to thank my family members for their greatest love and caring. Without their continuous support, I couldn't have today's achievement. I am, and will be deeply indebted to my family for my whole life.

April 16, 2013

ABSTRACT

NONINVASIVE ASSESSMENT OF TUMOR HYPOXIA USING OXYGEN SENSITIVE MRI IN PROSTATE TUMOR MODELS

RASHMI REDDY PABHATHI REDDY, M.S

The University of Texas at Arlington, 2013

Supervising Professor: Ralph P. Mason

A variety of solid tumors reveal oxygen deficiency as a result of rapid growth and insufficient tumor angiogenesis. Hypoxia in solid tumors appears to speed up malignant progression and metastatic potential of primary tumors thus leading to resistance against anticancer drugs and decreased response to radiotherapy.

Of various in vivo non-invasive techniques to assess tumor hypoxia, oxygen-sensitive MRI (BOLD and TOLD) is an attractive and reliable option. Blood Oxygen Level Dependent (BOLD) and Tissue Oxygen Level Dependent (TOLD) MRI offer potential insight into tumor hypoxia. BOLD (Blood Oxygen Level Dependant) contrast MRI which measures R_2* ($1/T_2$*) is sensitive to endogenous paramagnetic deoxyhemoglobin and TOLD (Tissue Oxygen Level Dependant) MRI which measures R_1 ($1/T_1$) is based on T_1-weighted imaging, which is sensitive to actual tumor tissue oxygenation. In this study, I investigate the efficacy of BOLD and TOLD to evaluate tumor hypoxia in response to oxygen challenge in rats.

All MRI experiments were performed on a 4.7T small animal Varian scanner. Variation in BOLD and TOLD signal response observed in syngeneic Dunning R3327-AT1 prostate tumor, with respect to oxygen breathing were compared with [^{18}F]-Fluoromisonidazole

(^{18}FMISO) PET in hypoxic regions. In addition, variation in BOLD and TOLD signal response in syngeneic Dunning R3327-H, -HI, -AT1, -MAT-Lu prostate tumor sublines with respect to oxygen breathing was examined. The dependence of BOLD and TOLD signal response on tumor size is investigated. Preliminary studies on orthotopic PC3 tumors were done to examine the efficacy of BOLD and TOLD contrast MRI to assess tumor hypoxia.

Significant correlations were found between BOLD and TOLD MRI and [^{18}F] FMISO PET measurements for oxygen breathing. Considerable correlations were found between oxygen sensitive MRI (BOLD and TOLD) and tumor size. Preliminary studies on orthotopic tumors yielded convincing results providing a potential approach to translate BOLD and TOLD contrast MRI for clinical translation.

TABLE OF CONTENTS

ACKNOWLEDGEMENTS iii

ABSTRACT iv

LIST OF ILLUSTRATIONS viii

LIST OF TABLES x

Chapter Page

1. INTRODUCTION 1

1.1 Tumor microenvironment 1

1.2 Tumor hypoxia 2

1.3 Magnetic Resonance Imaging 4

1.3.1 NMR Relaxation and pulse sequences 5

1.3.2 Oxygen Sensitive MRI (BOLD/TOLD) 7

1.3.3 Dynamic Contrast Enhanced MRI 9

1.4 Positron Emission Tomography (PET) 10

1.5 Overview of the study 11

2. EVALUATING TUMOR HYPOXIA USING BOLD MRI IN CORRELATION WITH [^{18}F]-FMISO PET IN DUNNING R3327-AT1 PROSTATE TUMOR BEARING RATS 12

2.1 Abstract 12

2.2 Introduction 13

2.3 Materials and Methods 14

2.3.1 Animal model 14

2.3.2 Tumor oximetry 14

2.3.3 MRI Data analysis 17

2.3.4 Radiochemicals 17

2.3.5 PET data acquisition and data analysis 18

2.3.6 Statistical analysis 19

2.3.7 Results 19

2.4 Discussion 28

2.5 Conclusion 29

3. ASSESSING TUMOR HYPOXIA USING BOLD AND TOLD CONTRAST MRI IN SYNGENEIC DUNNING PROSTATE TUMORS 31

3.1 Abstract 31

3.2 Introduction 31

3.3 Materials and Methods 32

3.3.1 Animal model 32

3.3.2 Tumor oximetry 33

3.3.3 Results 33

3.4 Discussion 40

3.5 Conclusion 41

4. PRELIMINARY STUDIES OF BOLD AND TOLD CONTRAST MRI IN PC3 ORTHOTOPIC PROSTATE TUMORS 42

4.1 Introduction 42

4.2 Materials and Methods 43

4.2.1 Animal model 43

4.2.2 Tumor oximetry 43

4.2.3 Dynamic Contrast Enhanced MRI 44

4.2.4 Results 44

4.3 Discussion 47

4.4 Conclusion and future directions 47

REFERENCES 49

BIOGRAPHICAL INFORMATION 54

LIST OF ILLUSTRATIONS

Figure Page

1.1 Scanning electron microscope images of vascular casts (a) Normal organized vasculature of colon tissue. (b) Disorganized vasculature of nearby colonic cancer.....2

1.2 Timing diagram of Spin echo sequence.....6

1.3 Timing diagram of Gradient echo sequence. 7

1.4 Time vs. contrast enhancement graph shows pattern of enhancement over time for various ROIs.....9

1.5 Co-registered CT and FMISO-PET images in transaxial, sagittal, and coronal slices of a patient with neck cancer 10

2.1 MRI data acquisition scheme.....16

2.2 Synthesis scheme of [^{18}F]1-(2-nitro-1-imidazolyl)-3-fluoro-2-propanol (^{18}FMISO) 18

2.3 Tumor heterogeneity in Rat # 4. (a) [^{18}F] FMISO uptake regions suggesting hypoxia. (b)BOLD response map with respect to oxygen challenge. (c) BOLD response map with respect to oxygen challenge. Low BOLD and TOLD response regions suggesting hypoxia..21

2.4 Figure 2.4 Immunohistochemistry- Hypoxia staining (a) Rat #4, (b) Rat #3, (c) Rat #5, (d) Rat #6 22

2.5 T_2* Decay curve of the tumor signal intensity as a function of echo time for Rat#2 for the whole tumor 24

2.6 Correlations between BOLD and TOLD responses of individual tumors. (a)Hypoxic region and (b) Whole tumor.....25

2.7 Correlations between BOLD and TOLD responses of individual tumors with ΔR_2* in hypoxic regions. (a) BOLD response to ΔR_2* (b) TOLD response to ΔR_2* 26

2.8 Correlations between BOLD and TOLD responses with Hypoxic region to muscle ratio (HR/M) of individual tumors. (a) Hypoxic region BOLD response to HR/M and (b) Hypoxic region TOLD response to HR/M 27

2.9 Correlation between ΔR_2*with Hypoxic region to muscle ratio (HR/M) of individual tumors in hypoxic region.....28

3.1 Oxygen sensitive MRI. (a) High resolution T_2-W image showing the tumor and muscle, (b) BOLD, (c) TOLD, (d) Changes in tumor oxygenation in response to oxygen breathing: mean changes in BOLD (blue) and TOLD (red) 35

3.2 Comparison of BOLD and TOLD response to oxygen challenge for 12 H, HI, AT1 and MAT-Lu tumors. Correlation of BOLD and TOLD based on mean change in signal intensity due to oxygen breathing 37

3.3 Comparison of BOLD response and mean change in transverse relaxation rates to oxygen challenge for 12 H, HI, AT1 and MAT-Lu tumors. Correlation of average change in BOLD and R_2* due to oxygen breathing 37

3.4 Comparison of TOLD response and mean change in transverse relaxation rates to oxygen challenge for 12 H, HI, AT1 and MAT-Lu tumors. Correlation of average change in TOLD and R_2* due to oxygen breathing 38

3.5 Comparison of BOLD response (% ΔSI) to tumor size (cm^3) 38

3.6 Comparison of TOLD response (% ΔSI) to tumor size (cm^3) 39

3.7 Comparison of mean change in transverse relaxation rate (ΔR_2*) to tumor size (cm^3) 39

3.8 Bar graph comparing BOLD, TOLD responses and R_2* in R3327-H, -HI, -AT1 and –MAT-Lu tumors. Mean changes in BOLD, TOLD responses and R_2* with standard deviation as error bars in individual sublines. Change in signal intensity of BOLD (%ΔSI) in blue, TOLD (%ΔSI) in red and mean changes in R_2* (ΔR_2*) in green 40

4.1 Oxygen sensitive MRI. (a) High resolution T_2-W image showing the tumor and muscle, (b) BOLD, (c) TOLD, (d) Changes in tumor oxygenation in response to oxygen breathing: mean changes in BOLD (blue) and TOLD (red) 45

4.2 Oxygen sensitive MRI. (a) High resolution T_2-W image showing the tumor (green) and muscle (red), (b) Contrast enhancement plot for 60 dynamic images 46

LIST OF TABLES

Table Page

1.1 Isotopes and NMR frequencies of major elements available in body 4

2.1 BOLD, TOLD responses, change in transverse relaxation rates in hypoxic region and corresponding uptake in hypoxic region to muscle ratio (HR/M) of individual Dunning prostate R3327-AT1 tumors 20

2.2 BOLD, TOLD responses, baseline transverse relaxation rates (air), change in transverse relaxation rates in hypoxic regions and whole tumor of individual Dunning prostate R3327-AT1 tumors. 23

2.3 [^{18}F] FMISO uptake in Hypoxic regions (HR), Whole tumor (WT), Muscle (M), Hypoxic region to muscle ratio (HR/M), Whole tumor to muscle ratio (WT/M) individual Dunning prostate R3327-AT1 tumors 24

3.1 Effect of oxygen breathing on BOLD and TOLD MRI and R_2* of Dunning prostate R3327-H, -HI, -AT1 and –MAT-Lu tumors 36

CHAPTER 1

INTRODUCTION

1.1 Tumor microenvironment

Cancer is the uncontrolled growth of abnormal cells in the body. In most cases, this uncontrolled cell growth causes the formation of tumors, either solid or dispersed [1]. There are over 200 different known cancers in man. Cancer can be detected in a number of ways, including the presence of certain signs and symptoms, screening tests, or medical imaging. Untreated cancers can cause serious illness by invading healthy tissues and lead to death. Cancer is usually treated with chemotherapy, radiation therapy and surgery.

A neoplasm can be caused by abnormal proliferation of tissues in the body, which can be caused by genetic mutations. However, it is not necessary that all types of neoplasm cause a tumorous overgrowth of tissue. A tumor may be either benign or malignant. Benign tumors are self-contained, non-lethal, and grow more slowly than malignant ones. Malignant tumors are cancerous growths which expand quickly and can metastasize, or spread to other areas of the tissue or body. Malignant tumors grow by invading nearby cells and spread to other parts of the body through a process called metastasis.

The study of the microenvironment includes normal cells and molecules that surround a tumor cell. It describes the physiological and metabolic conditions within solid tumors and is different from that of normal tissues [2]. According to Swartz et al., the tumor microenvironment (TME) consists of cells, soluble factors, signaling molecules, extracellular matrix and mechanical cues that promotes neoplastic transformation and supports tumor growth and invasion [1]. TME plays a crucial role in carcinogenesis and metastasis thereby making it an

important factor for cancer therapy. New modalities are being developed to study and target tumor microenvironment.

1.2 Tumor hypoxia

Inadequate supply of oxygen results in tumor hypoxia. Tumor hypoxia appears to be strongly associated with tumor propagation, malignant progression, and resistance to therapy [2]. Major factors that cause tumor hypoxia are abnormal structure and function of the micro-vessels supplying the tumor, increased diffusion distances between the nutritive blood vessels and the tumor cells, and reduced oxygen transport capacity of the blood [3]. Tumor hypoxia results in poor outcome of radiotherapy since hypoxic cells are relatively radio-resistant compared with normal cells [4]. Tumor vasculature is created through cooption of normal vasculature due to the replacement of normal tissue with abnormal cells, and angiogenesis which is formation of new blood vessels from pre-existing vessels [5]. The abnormal vasculature of tumor is compared to the normal vasculature in the figure below.

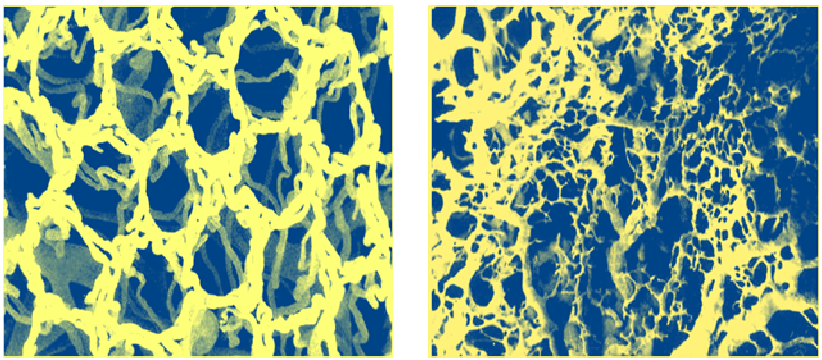

Figure 1.1 Scanning electron microscope images of vascular casts. (a) Normal organized vasculature of colon tissue. (b) Disorganized vasculature of nearby colonic cancer. (Figure adapted from [6])

Tumor tissues may be characterized by the presence of three types of hypoxia, which are related to perfusion, diffusion and anemia [2]. Perfusion related hypoxia also known as acute hypoxia is a result of inadequate blood flow in tissues. This is due to severe structural and functional abnormalities of tumor vasculature which include disorganized vascular network,

dilations, an elongated and tortuous shape, an incomplete endothelial lining, a lack of physiological/pharmacological receptors, an absence of flow regulation, and intermittent stasis. This can also lead to ischemic hypoxia, which is often transient [2]. Diffusion related hypoxia also known as chronic hypoxia is a result of increase in diffusion distances with tumor expansion which leads to inadequate oxygen supply for cells distant from the nutritive blood vessels [2]. Anemic hypoxia is a result of reduced oxygen transport capacity of the blood subsequent to tumor-associated or therapy-induced anemia. Low hemoglobin levels (10-12 g/dl) lead to reduced oxygen supply to tumors thereby intensifies hypoxia [2, 7].

To detect hypoxia, there are many methods available which can be broadly classified into *in vitro* and *in vivo*. In vitro techniques include immunohistological techniques or enzymatic assays to detect hypoxia. Though they are accurate, they are invasive requiring tissue samples and can be performed only on a small sample which cannot give a global picture of oxygenation of the whole tumor. *In vivo* studies use a combination of both anatomical and functional imaging to provide a more complete picture of morphology, extent and grade of tumor along with biological and molecular characteristics. I*n vivo* methods of assessing tumor hypoxia may be more or less invasive. Polarographic microelectrode measurement is an invasive method where an electrode is inserted into the solid tumor to measure the oxygen concentrations. Non-invasive methods are more attractive due to reduced risk factors and complexity. Fluorescence probes, positron emission tomography (PET), single photon emission computed tomography (SPECT), magnetic resonance imaging (MRI), electron paramagnetic resonance spectroscopy (EPR), near-infrared spectroscopy (NIRS) have each been demonstrated as non-invasive hypoxia assessing methods [8, 9]. Of these various techniques, MRI and PET are of primary interest in my study.

1.3 Magnetic Resonance Imaging

Magnetic resonance imaging has emerged as a powerful imaging technique in the medical field because of its high resolution capability in viewing internal structures of the body. It uses magnetic fields and radio frequency signals to obtain anatomical information as cross-sectional images of the body in any desired direction and can easily discriminate between healthy and diseased tissue.

When a sample is placed in a magnetic field B_0, the randomly oriented nuclei experience an external magnetic torque, which tends to align the individual parallel or anti-parallel magnetic moments to the direction of an applied magnetic field. There is a slight excess of nuclei aligned parallel with the magnetic field and this gives the tissue a net magnetic moment M_0. According to the electromagnetic theory, any nucleus such as a hydrogen proton, which possesses a magnetic moment attempts to align itself with the magnetic field and can absorb energy in the radiofrequency range. When changed to the original state, it re-emits the absorbed energy. The NMR frequencies and other characteristics of some of the common biological isotopes are given in table 1-1.

Table 1.1 Isotopes and NMR frequencies of major elements available in body

Element	% of body weight	Isotope	NMR frequency (MHz/T)
Hydrogen	10	^{1}H	42.57
Carbon	18	^{13}C	10.7
Nitrogen	3.4	^{14}N	3.08
Sodium	0.18	^{23}Na	11.26
Phosphorous	1.2	^{31}P	17.24

The three basic components required for MRI are a superconducting magnet, RF transmitter-receiver coil and gradient coils. The superconducting magnet provides a strong, uniform, steady magnetic field. Four factors that characterize the performance of the magnets used in MR systems are field strength, temporal stability, homogeneity and bore size. Most of

the modern MRI systems utilize superconductive magnets that are maintained at a very low temperature (about 4.2 Kelvin) using cryogens in order to reduce the electrical resistance.

The RF coils can be either a single coil serving as both transmitter and receiver or two separate coils that are electrically orthogonal. In both cases, all coils generate RF fields orthogonal to the direction of main magnetic field. Leach *et al*., 1986 discussed the design of special RF coils for various applications along with the physical and anatomical criteria responsible for the required shapes and forms [10]. Some of the commonly available coils are body coils, head coils, surface coils and organ-enclosing coils.

Spatial distribution information can be obtained by using the fact that the resonance frequency depends on the magnetic field strength. In MRI systems, for spatially resolving the signals emitted by the object, the initially homogenous magnetic field B0 is overlaid in all three spatial dimensions X, Y, Z with small linear magnetic fields-gradient fields G. These gradient fields can be switched on or off as desired, both during the application of the RF energy and also in any phase of the measuring procedure. The main purpose is to cause the MR signal to become spatially dependent.

1.3.1 NMR Relaxation and pulse sequences

When a sample of water is introduced into a magnetic field, B_0, the nuclear spins precess about B_0 along the direction of the field. Excitation by an RF pulse causes the nuclear spins to change from low to high energy states. This is followed by spontaneous relaxation, where the magnetization returns to its equilibrium configuration. Recovery along the longitudinal plane of B0 is called T_1 relaxation and along the transverse plane is called T_2 relaxation.

Longitudinal (T_1) relaxation also termed as spin-lattice relaxation refers to the return of longitudinal magnetization to its ground state. Transverse (T_2) relaxation, also termed as spin-spin relaxation is the process by which the magnetization in the transverse plane loses its

phase coherence. T_2* relaxation is the loss of signal seen with dephasing of individual magnetizations and it corresponds to the inhomogeneities in the magnetic field.

An MRI sequence is an ordered combination of RF and gradient pulses designed to acquire the data to form the image. The essential elements in designing a pulse sequence are RF pulse, phase encoding, frequency encoding/readout. The two basic sequences used in the study are spin echo and spoiled gradient echo.

- Spin Echo Sequence

Initially, all the spins are stationary on an average. A 90^o excitation pulse is applied to flip the magnetization to horizontal plane (x-y). Due, to the magnetic inhomogeneities, there is a decay of signal. This is followed by 180^o pulse to refocus the spins and a signal echo is generated. In a standard spin echo sequence, applying short TR and short TE produces a T_1 -weighted image since the spins do not have sufficient time to full relax between excitations. Long TR and long TE produce a T_2-weighted image. T_2*-weighted images cannot be generated using a 180^o refocusing pulse [11]. The signal from a spin echo is as follows where ρ is the density of spins in the sample:

$$S = k\rho(1-e^{-TR/T1})e^{-TE/T2}$$

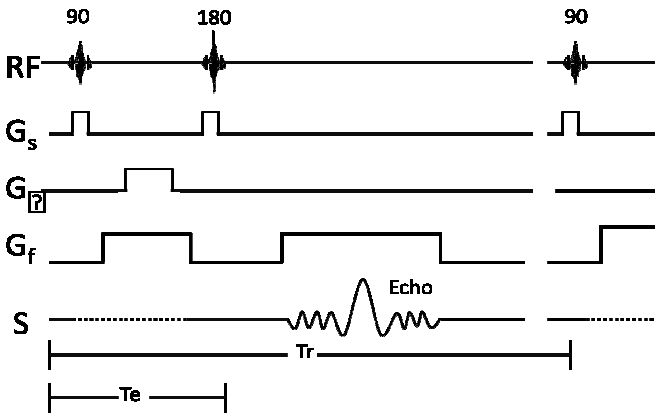

Figure 1.2 Timing diagram of Spin echo sequence (RF: radiofrequency; G_s: slice selection; Gφ: phase encoding; G_f: frequency encoding; S: signal intensity)

- Spoiled Gradient Echo Sequence

Unlike spin echo sequence, Gradient Echo Sequence consists of a single 90^o excitation pulse. The flip angle for a spin echo sequence is close to 90^o and for a gradient echo sequence; it varies from 0^o to 90^o. In certain cases, the gradients and RF pulses are used to eliminate transverse magnetization called as spoiled gradient echo which particularly is used in my studies. The image contrast depends on flip angle, TR and TE. The signal intensity is given by the equation mentioned below [12].

$$S = \frac{M_0 \sin\theta(1 - e^{-TR/T1})}{1 - \cos\theta\, e^{\frac{-TR}{T1}}} e^{-TE/T2^*}$$

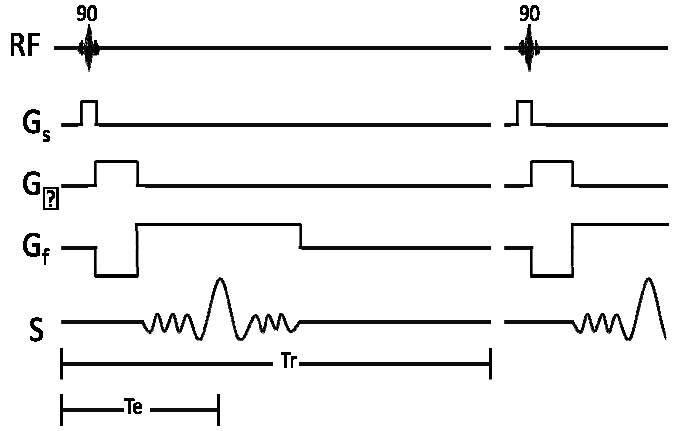

Figure 1.3 Timing diagram of Gradient echo sequence (RF: radiofrequency; Gs: slice selection; Gφ: phase encoding; Gf: frequency encoding; S: signal intensity)

1.3.2 Oxygen sensitive MRI (BOLD/TOLD)

In a healthy human being, approximately 98.5% of the oxygen in arterial blood is chemically combined with hemoglobin and about 1.5% is dissolved in blood plasma. It was found in the 1930s that hemoglobin has magnetic properties that are different depending on whether it is carrying oxygen or not. Deoxy-hemoglobin (dHb) possesses paramagnetic properties whereas oxygenated hemoglobin (Hb) possesses diamagnetic properties. These

magnetic properties allow blood to be used as an important endogenous agent to evaluate oxygenation noninvasively using MRI [12]. As MRI uses a very strong magnetic field, this difference in the magnetic properties of oxygenated and deoxygenated hemoglobin in blood can be detected as so-called the BOLD (blood oxygenation level dependent) contrast. The paramagnetic nature of deoxy-hemoglobin influences T_2* relaxation. TOLD (tissue oxygen level dependent) is the T_1 effect of dissolved oxygen in the tissue and blood plasma and it provides a mechanism of monitoring tissue oxygenation (pO_2) [13].

In BOLD (Blood Oxygen Level Dependent) MRI studies, change of transverse relaxation rate R_2* ($1/T_2$*) and response to oxygen breathing (ΔSI) are of interest [14, 15]. Though it is suggested that higher R_2* values reflect hypoxia, it also depends on B0 field inhomogeneity, changes in blood flow and blood volume, hemorrhage, vascular structure, calcification and iron deposition in the tissue [16-18]. Tumor oxygenation can be studied by response to hyperoxic gas breathing, revealed by changes in R_2* and contrast in T_2*-weighted images [19-26].

TOLD (Tissue Oxygen Level Dependent) MRI is based on spoiled gradient echo T_1 relaxation time measurements or T_1-weighted images. It is more directly related to tissue pO_2 compared to BOLD MRI as it is based on availability of oxygen dissolved in blood plasma or interstitial space in the tissue. The extent of interstitial volume and regional blood flow and oxygen consumption influences the T_1 response to oxygen inhalation in various tissues [16, 27-29] whereas T_2* depends on signal loss induced by local magnetic fields inhomogeneities.

Hence, the combination of BOLD and TOLD MRI provides a better understanding of tumor oxygenation as it gives the quantitative representation of tumor hypoxia. As non-invasive quantitative analysis of tumor hypoxia is of interest in recent research studies, BOLD and TOLD MRI provides a robust insight to it.

1.3.3 Dynamic contrast enhanced MRI

Dynamic contrast enhanced MRI is a conventional method used in clinical scans to examine tumors. As the name suggests, it is a dynamic study where fast MRI is done before, during, and after the rapid intravenous administration of a gadolinium-based contrast agent, providing functional information. This technique is also sensitive to physiological and morphological properties [30-33]. In solid tumors, there is a rapid and intense contrast enhancement followed by a relatively rapid washout in normal tissues [34]. The amount of injected contrast agent is standardized based on the subject's body weight.

On T_1-weighted images, signal intensity enhancement patterns can be evaluated using two techniques, semi-quantitative and quantitative methods [34]. In the semi-quantitative method, the signal intensity vs. time curve is determined [25]. This determines how the signal is enhanced with respect to the baseline signal intensity. However, as it also depends on scanning conditions, pre-contrast a T_1 map of tissues is required to convert signal intensity to Gd concentration. Quantitative techniques use pharmacokinetic models to calculate permeability constants [35].

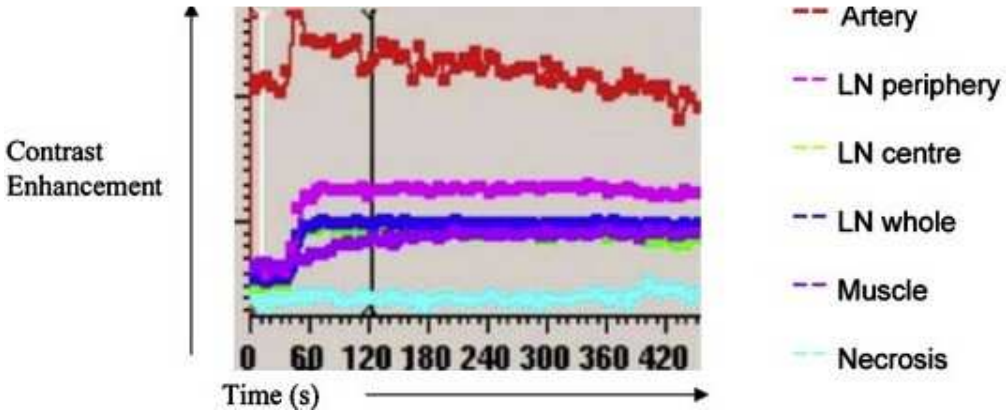

Figure 1.4 Time vs. contrast enhancement graph shows pattern of enhancement over time for various ROI. LN indicates Lymph node (adapted from [30])

1.4 Positron Emission Tomography (PET)

Positron Emission Tomography is a type of nuclear medicine imaging that uses a radioactive substance called a tracer to study the functioning of organs and tissues in the body. The tracer is injected intravenously and travels through the blood and collects in tissues and organs of the body. It produces 3-dimensional images of the functional processes within the body. A PET scan can reveal vital body functions, such as blood flow, oxygen use and sugar metabolism. In recent studies, combined PET and CT scanners are used to provide anatomical context for the radionuclide uptake. PET is increasingly used to evaluate patients with known or suspected cancer particularly to reveal metastasis. Most investigations use [^{18}F]fluorodeoxyglucose (FDG) as a tracer, which shows high uptake in cancerous lesions and low uptake in benign lesions giving a good scope for both sensitivity and specificity [36]. An alternate PET tracer, [F-18] fluoromisonidazole (FMISO) is being used to study hypoxia in tumors in various parts of the body [37, 38]. Head and neck cancer showed accumulation of [F-18] FMISO indicating hypoxia as studied by Hendrickson, *et al*. [37].

Figure 1.5 Co-registered CT and FMISO-PET images in transaxial, sagittal, and coronal slices of a patient with neck cancer (adapted from [37])

Dukart et al., showed substantial gain in accuracy using combined FDG-PET and MRI to detect dementia [38]. An integrated study of FMISO-PET and MRI was used by Szeto et al., for quantitative assessment of diagnosed glioblastoma [39]. As both PET and MRI studies are non-invasive, they offer a potential use in present research to assess tumor hypoxia which is discussed in my study.

1.5 Overview of the study

Previous studies showed that radiotracers selectively accumulate in hypoxic tumors, which can be applied together with functional PET or SPECT imaging. It can be used to look at the hypoxic regions in a tumor. Among the potential PET hypoxia tracers, ^{18}F-labeled 1-(2-nitro-imidazolyl)-3-fluoro-2-propanol ([^{18}F]-Fluoromisonidazole (^{18}FMISO) is the most widely used PET radiotracer for imaging tumor hypoxia. My goal was to apply oxygen sensitive MRI (BOLD and TOLD) with respect to oxygen gas challenge as potential surrogate biomarkers for tumor oxygenation. BOLD contrast MRI, which measures R_2* ($1/T_2$*), is sensitive to endogenous paramagnetic deoxyhemoglobin and TOLD MRI, which measures R_1 ($1/T_1$), is based on T_1-weighted imaging and is sensitive to actual tumor tissue oxygenation. I examined variation in BOLD and TOLD signal response in syngeneic Dunning R3327-AT1 prostate tumors, with respect to oxygen breathing and compared results with [^{18}F]-Fluoromisonidazole (^{18}FMISO) PET uptake to examine the hypoxic regions of the tumor quantitatively. My fundamental hypothesis was that PET and MRI techniques would provide consistent information for assessing tumor hypoxia (Chapter 2).

In addition, variation in BOLD and TOLD signal response in syngeneic Dunning R3327-H, -HI, -AT1, -MAT-Lu prostate tumor sublines with respect to oxygen breathing was examined in Chapter 3. These four tumor sublines are reported to exhibit different characteristics based on metastasis, growth, differentiation and pathophysiology. My goal was to examine differences or similarities in tumor oxygenation based on the oxygen sensitive MRI. My hypothesis was that BOLD and TOLD signal response would depend on tumor size, but be independent of tumor type.

In addition to the subcutaneous tumor studies, preliminary studies on orthotopic PC3 tumors were performed to examine the efficacy of BOLD and TOLD contrast MRI to assess tumor hypoxia in Chapter 4, followed by conclusion and future directions of my study.

CHAPTER 2

EVALUATING TUMOR HYPOXIA USING BOLD MRI IN CORRELATION WITH [^{18}F]-FMISO PET IN DUNNING R3327-AT1 PROSTATE TUMOR BEARING RATS

2.1 Abstract

The aim of the study was to compare oxygen sensitive MRI (BOLD and TOLD) in Dunning prostate R3327-AT1 tumor bearing rats with [^{18}F]-fluoromisonidazole ([^{18}F] FMISO), which is a widely used PET radiotracer for imaging tumor hypoxia[40, 41]. Dunning prostate R3327-AT1 tumor bearing rats (1.4 to 2.6 cm^3) were examined with respect to oxygen breathing challenge using interleaved BOLD (T_2*-weighted) and TOLD (T_1-weighted) sequence, which is sensitive to paramagnetic deoxyhemoglobin and tumor tissue oxygenation (pO_2) respectively. The following day, the administration (570-600 µCi) of the radio tracer via tail vein, dynamic PET imaging was performed up to 90 min using a Siemens Inveon® PET/CT system. The 0-90 min imaging data were reconstructed into eighteen frames, where each frame represented the average value of the respective 5 min interval and the time activity curve was generated. Each technique showed heterogeneity in tumors. PET imaging showed maximum [^{18}F] FMISO uptake in the peripheral regions and MRI showed lower BOLD and TOLD response in the same region consistent with hypoxia. The results were further verified by performing immunohistochemistry on the tumor tissue. Pimonidazole accumulating in hypoxic regions and Hoechst 33342 stain in well perfused regions were observed. Immunohistochemistry confirmed the presence of hypoxic regions.

2.2 Introduction

A variety of solid tumors exhibits oxygen deficiency as a result of rapid growth and insufficient angiogenesis. Hypoxia in solid tumors appears to speed up malignant progression and metastatic potential of primary malignomas thus leading to resistance against anticancer drugs and decreased response to radiotherapy. To date, the invasive technique of using computerized polarographic oxygen-sensitive electrodes is regarded to be the gold standard for measuring the hypoxic fraction in tumors [19, 42]. However, the search for a non-invasive approach to detect tumor hypoxia is still a big challenge. The most encouraging results have been obtained using radiotracers that selectively accumulate in hypoxic tumors and which can be applied together with functional PET or SPECT imaging. Also, Magnetic Resonance Imaging (MRI) is regarded as another non-invasive technique that offers an impending approach to assess tumor hypoxia [43].

Among the potential PET hypoxia tracers, ^{18}F-labeled 1-(2-nitro-imidazolyl)-3-fluoro-2-propanol ([^{18}F]-Fluoromisonidazole (^{18}FMISO) is the most widely used PET radiotracer for imaging tumor hypoxia [44]. Meanwhile Oxygen sensitive MRI is an attractive alternative option. Blood Oxygen Level Dependent (BOLD) and Tissue Oxygen Level Dependent (TOLD) MRI offer potential insight into tumor hypoxia. BOLD (Blood Oxygen Level Dependant) contrast MRI which measures R_2* ($1/T_2$*) is sensitive to endogenous paramagnetic deoxyhemoglobin and TOLD (Tissue Oxygen Level Dependant) MRI which measures R_1 ($1/T_1$) is based on T_1-weighted imaging, which is sensitive to actual tumor tissue oxygenation [19, 43, 45, 46]. The responses to oxygen challenge were tested and compared with a PET tracer that binds to the hypoxic region [44].

It is the aim of my study to quantitatively compare hypoxia dependent uptake of [^{18}F]-FMISO in subcutaneous rat tumors, as registered noninvasively with PET. Of various invasive and non-invasive imaging techniques used to assess tumor hypoxia, oxygen sensitive Magnetic Resonance Imaging has shown promising results [20, 22, 47-49]. Blood Oxygen Level

Dependent (BOLD) and Tissue Oxygen Level Dependent (TOLD) MRI offer potential insight into tumor hypoxia and are compared here with [F-18] fluoromisonidazole (^{18}F-FMISO), an established PET tracer to detect and image hypoxia in my study. The hypothesis of this study is that combining MRI and PET provides complimentary information to assess tumor hypoxia.

2.3 Materials and methods

2.3.1. Animal model

This study was approved by the Institutional Animal Care and Use Committee. Dunning prostate R3327-AT1 adenocarcinoma was selected. Six male Copenhagen rats were implanted subcutaneously with Dunning R3327-AT1 tumor. AT1 is an anaplastic, low metastatic, comparatively fast growing tumor subline with tumor volume doubling time of 5.2 days[50]. Tumors were originally obtained from Dr. J. T. Isaacs (Johns Hopkins, Baltimore, MD) [51] and provided to us by Dr. P. Peschke (DKFZ, Heidelberg, Germany). Tumors were implanted in adult male Copenhagen-2331 rats. Tumors were allowed to grow (1.4 to 2.6 cm^3) and were investigated by magnetic resonance imaging (MRI). For MRI, the rats were maintained under general gaseous anesthesia (1.5% isoflurane in air (1 L/min); Baxter International, Deerfield, IL) and kept warm (37 ℃) using a circulating warm wate r blanket.

2.3.2. Tumor oximetry

MRI was performed at 4.7T MRI using a single turn solenoid coil tunable to ^{1}H and ^{19}F. Six rats bearing SC Dunning prostate R3327-AT1 tumors were examined with respect to oxygen breathing challenge using interleaved BOLD (T_2* weighted) contrast which is sensitive to paramagnetic deoxyhemoglobin and TOLD (T_1 weighted) sensitive to tumor tissue oxygenation (pO_2). High resolution T_2-weignted anatomical images were acquired using Fast spin echo sequence (TR=2000 ms, effective TE=48ms, Echo Train Length (ETL) = 8, 128X128

data matrix, 40X40 mm FOV, 1 mm slice thickness without gap). Interleaved BOLD and TOLD sequence (IBT) with baseline (air) followed by oxygen challenge was run. BOLD used Multi-echo Gradient Echo (TR=150 ms, 10 echo times TE=6-69 ms with echo spacing of 7 ms, flip angle (FA) = 20°, acquisition time 21 s. 128X128 da ta matrix, 40X40 mm FOV) and TOLD uses Gradient Echo sequence (TR=30 ms, TE=5 ms, flip angle (FA) = 45°, acquisition time 3 seconds, 128X128 data matrix, 40X40 mm FOV). The following day, [F-18] fluoromisonidazole was successfully synthesized and injected via tail vein. Dynamic PET was performed up to 90 min post injection using an Inveon preclinical PET/CT scanner, and the time activity curve was generated.

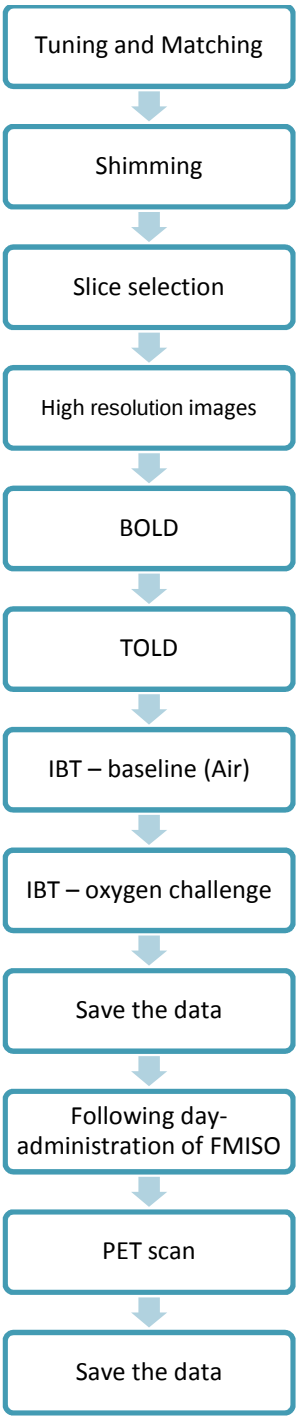

Figure 2.1 Data acquisition scheme.

2.3.3 MRI Data analysis

MRI data were processed using Matlab (MathWorks Inc., Natick, MA) scripts written by Dr. Rami Hallac. Regions of interest (ROIs) were taken based on the hypoxic regions determined by PET. By manual comparison, high signal intensity regions in PET corresponded to low BOLD and TOLD response regions in MRI. The ROIs were hence drawn on the low response regions of BOLD and TOLD maps generated by MRI. Changes in Signal Intensity (%ΔSI) with respect to oxygen challenge were calculated as

$$\Delta SI = \frac{SI_t - SI_b}{SI_b} \cdot 100\%$$

Where SI_b is the mean baseline signal intensity during air breathing and SI_b is the mean signal intensity with oxygen inhalation.

R_2* (1/ T_2*) maps were generated by fitting the multi-echo T_2*W image signal intensity (MGEMS) to TE, as a single exponential function on a voxel-by-voxel basis. The change of R_2* or T_2* due to oxygen/carbogen challenge was then calculated as:

$$\Delta R_2^* = R_2^*t - R_2^*b$$

2.3.4 Radiochemicals

The radio tracer used in this study is [^{18}F]-fluoromisonidazole ([^{18}F] FMISO), a lipophilic compound that enters cells by diffusion. Under normoxic conditions, there is equilibrium of intra-cellular and extra-cellular FMISO while under hypoxic conditions, a sequence of single electron reduction takes place and it binds to intracellular macro molecules. Zimny *et al*. and few other groups found that there is retention of FMISO based on tissue oxygenation as assessed by pO_2-polarography [52-54]. Hence, the accumulation of FMISO in tumors is related to hypoxia.

Synthesis of [^{18}F]1-(2-nitro-1-imidazolyl)-3-fluoro-2-propanol (^{18}FMISO) [55].

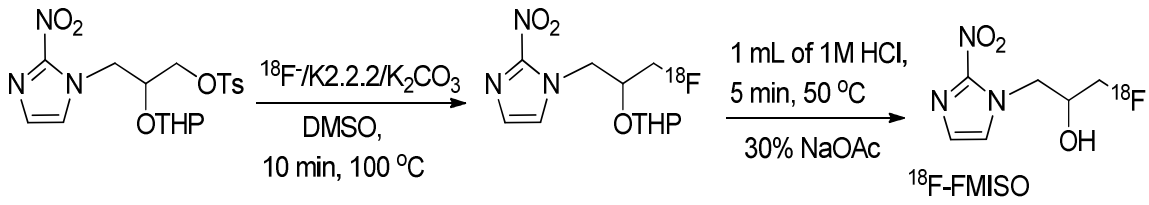

*F*igure 2.2 Synthesis scheme of [^{18}F]1-(2-nitro-1-imidazolyl)-3-fluro-2-propanol (^{18}FMISO)

2.3.5. PET data acquisition and data analysis

The imaging studies were performed on a Siemens Inveon Multimodality PET/CT (Siemens Medical Solution Inc., Knoxville, TN, USA). Ten minutes prior to imaging, the animals were anesthetized using 3% isoflurane at room temperature until stable vitals were established. Once the animal was sedated, the animal was placed onto the imaging bed under 2% Isoflurane anesthesia for the duration of the imaging.

The CT imaging was acquired at 80 kV and 500 µA with a focal spot of 58 µm. The total rotation of the gantry was 360^{o} with 360 rotation steps obtained at an exposure time of approximately 180ms/frame. The CT images were reconstructed with a down sample factor of 2 using Cobra Reconstruction Software. The PET imaging was acquired directly following the acquisition of CT data. Each AT1 prostate tumor bearing rat was injected with 570-600 µCi of ^{18}FMISO in 200 µl of saline via tail vein. Immediately after the injection, a dynamic PET scan was performed from 0 to 90 min. The 0-90 min dynamic imaging data were reconstructed into 18 frames (5 min each frame), where each frame represent the average value of the respective 5 min interval.

Reconstructed CT and PET images were fused and analyzed using Inveon Research Workplace (IRW) software. For quantification, regions of interest were placed in the specific areas, for example periphery, whole tumor, and highest activity of ^{18}FMISO region and muscle of contralateral thigh region determined by PET and guided by visual inspection of CT images.

The ratio of uptake of [^{18}F] FMISO (%ID/g) of the region where there was highest uptake of [^{18}F] FMISO to the muscle gives the hypoxic fraction of the tumor. This hypoxic fraction was compared to the percentage change in signal intensity of BOLD and TOLD with respect to oxygen challenge.

2.3.6 Statistical Analysis

For each ROI, mean baseline SI of the T_2*W images was calculated and compared with SI during O_2 challenge. An average of all data points was used to determine the response to oxygen challenge. Student's t-test was used to see the significance. R^2 value determines the correlation of these two methods.

2.3.7. Results

Mean change in signal intensity (% ΔSI) for BOLD, TOLD and %ΔR_2* were calculated for all six AT1 tumors. During oxygen challenge, various changes were observed with respect to baseline values. There was an increase in BOLD ΔSI and TOLD ΔSI and decrease in ΔR_2* when whole tumor was considered. The values of the whole tumor for the group of six tumors were observed to be BOLD ΔSI = 3.37±1.35%, TOLD ΔSI =1.85±1.17%, and ΔR_2*= -2.93±2.58 s^{-1}. When the ROI was taken across the low response region in BOLD and TOLD which corresponded to higher uptake region in [^{18}F] FMISO PET, the responses were found to be smaller than for the whole tumor. The mean values were observed to be BOLD ΔSI = -0.89±1.61%, TOLD ΔSI =0.08±0.31%, and ΔR_2*= -1.37±4.17 s^{-1}. Data for individual tumor are summarized in Table 2-1.

For PET analysis, when the whole tumor is considered, the average uptake in all tumors was observed to be 0.4±0.09%ID/g. When ROI is taken at highest uptake regions, which was considered as hypoxic region, the average uptake was observed to be 0.66±0.17% ID/g. When ROI is taken in the muscle region, the average response was observed to be 0.25±0.09

%ID/g. A ratio of values obtained at highest uptake regions to the muscle is taken which is considered to be hypoxic fraction with respect to the muscle (baseline values) for each tumor and the average value was observed to be 3.55±2.82 and whole tumor to muscle ratio is observed to be 1.96±1.45.

Correlation graphs were plotted for comparison of hypoxic regions, BOLD ΔSI vs. TOLD ΔSI, BOLD ΔSI vs. HR/M, TOLD ΔSI vs. HR/M, ΔR_2* vs. HR/M and the values were observed to be 0.90, 0.89, 0.85, 0.71 and corresponding p-values to be 0.01, 0.02, 0.02, 0.002 (all values <0.05) respectively, which shows that there is a very good correlation between the two methods while comparing the hypoxic regions. For comparing BOLD ΔSI vs. HR/M, TOLD ΔSI vs. HR/M, ΔR_2* vs. HR/M, exponential graphs appeared to be more relevant based on the scatter plot. Data obtained from MRI and PET is summarized individually for each tumor in Table 2.2 and 2.3 respectively.

Table 2.1 BOLD, TOLD responses, change in transverse relaxation rates in hypoxic region and corresponding uptake in hypoxic region to muscle ratio (HR/M) of individual Dunning prostate R3327-AT1 tumors.

Rat #	Size (cm^3)	BOLD (%ΔSI)	TOLD (%ΔSI)	ΔR_2*(s^{-1})	HR/M
1	2.0	-3.22±1.22	-0.30±2.11	2.97±1.25	8.56
2	1.3	-1.93±2.06	-0.25±3.33	2.77±2.56	5.28
3	2.0	0.05±3.22	0.15±1.23	-3.22±4.23	1.61
4	2.6	-1.59±1.23	0.04±1.45	0.89±2.89	2.50
5	1.4	1.02±1.89	0.50±2.34	-4.56±4.74	1.59
6	1.4	0.32±1.65	0.33±1.34	-7.08±5.65	1.77
Mean ± SD		-0.89±1.61	0.08±0.31	-1.37±4.17	3.55±2.82

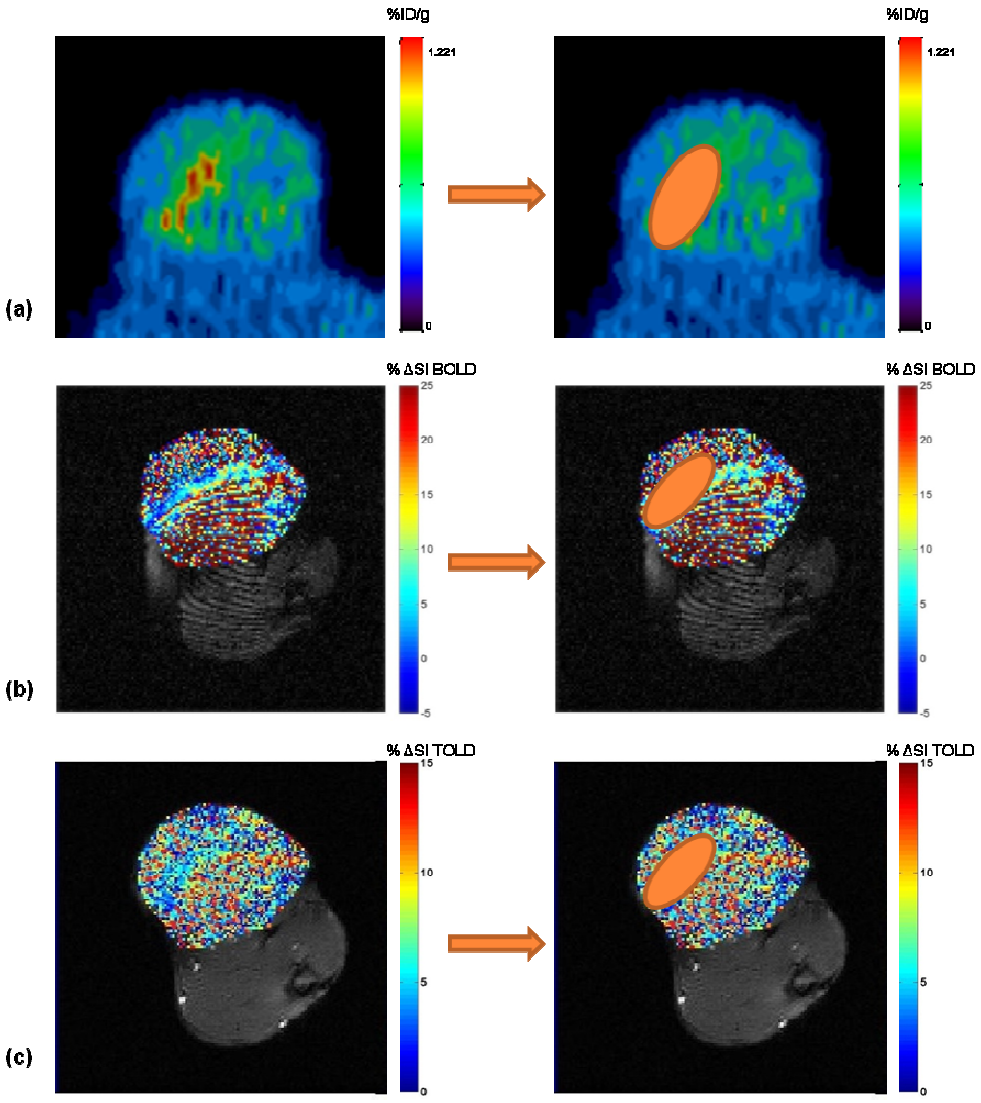

Figure 2.3 Tumor heterogeneity in Rat # 4. (a) [^{18}F] FMISO uptake regions suggesting hypoxia. (b) BOLD response map with respect to oxygen challenge. (c) TOLD response map with respect to oxygen challenge. Low BOLD and TOLD response regions suggesting hypoxia.

From Figure 2-3, the uptake of [^{18}F] FMISO at 90min PET scan is shown and the region of high signal corresponds to the high uptake. Respective BOLD and TOLD maps show low signal in the same regions. This confirms that high uptake regions of [^{18}F] FMISO PET correspond to low BOLD and TOLD response regions of MRI. BOLD and TOLD responses were plotted and explained in Chapter 3.

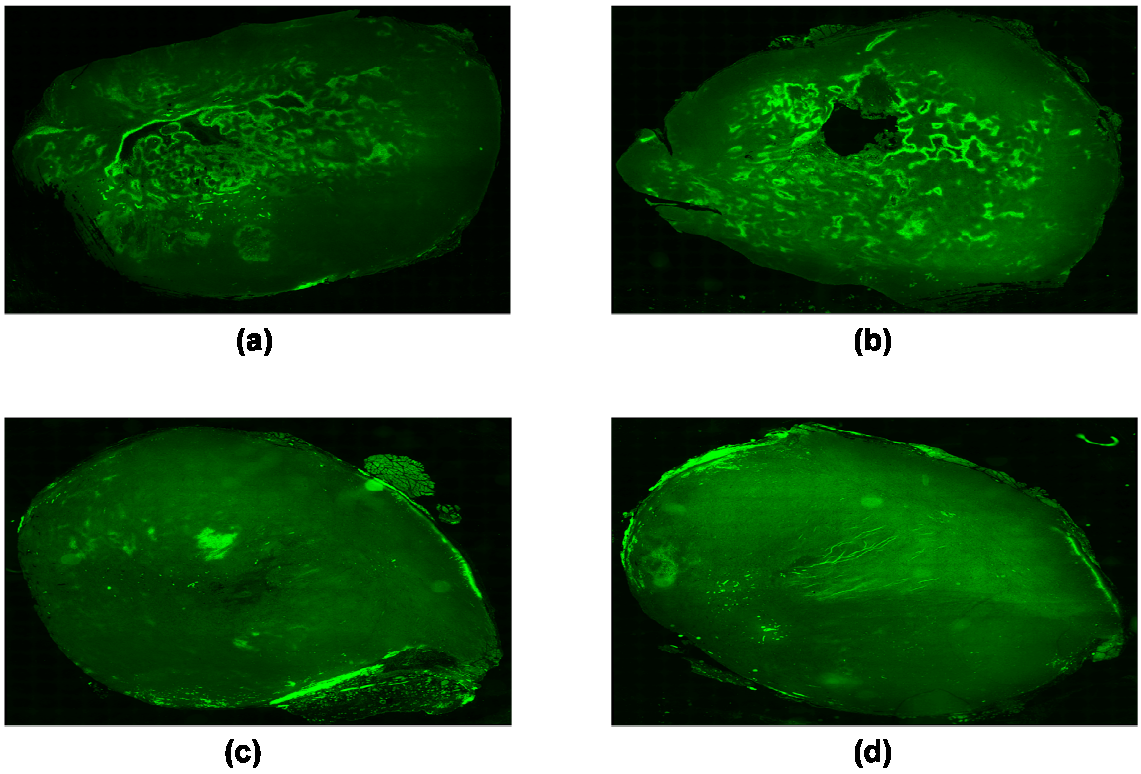

Figure 2.4 Immunohistochemistry- Hypoxia staining (a) Rat #4, (b) Rat #3, (c) Rat #5, (d) Rat #6

Figure 2.4 shows the results of immunohistochemistry done on four different tumors namely Rat#4, Rat#3, Rat#5, and Rat #6. Hypoxia staining was done on these four tumors and the bright regions in the images shows corresponding hypoxic regions which closely correlates to the data obtained using MRI and [^{18}F] FMISO PET. These regions correlated to the high uptake regions of [^{18}F] FMISO and low BOLD and TOLD response regions from MRI.

Table 2.2 BOLD, TOLD responses, baseline transverse relaxation rates (air), change in transverse relaxation rates in hypoxic regions and whole tumor of individual Dunning prostate R3327-AT1 tumors.

Rat #	Size (cm^3)	Hypoxic region BOLD %ΔSI	Whole tumor BOLD %ΔSI	Hypoxic region TOLD %ΔSI	Whole tumor TOLD %ΔSI	Hypoxic region R_2*(s^{-1}) - air	Whole tumor R_2* (s^{-1}) - air	Hypoxic region ΔR_2* (s^{-1})	Whole tumor ΔR_2* (s^{-1})
1	2	-3.22±1.22	0.37±1.83	-0.30±2.11	1.74±3.22	28.23±1.34	31.22±4.55	2.97±1.25	-0.15±3.26
2	1.3	-1.93±2.06	2.25±2.34	-0.25±3.33	1.40±3.22	32.14±2.36	35.16±3.78	2.77±2.56	-6.89±3.12
3	2	0.05±3.22	-0.46±1.89	0.15±1.23	3.87±4.56	28.78±1.96	30.41±5.65	-3.22±4.23	1.56±2.12
4	2.6	-1.59±1.23	4.22±4.53	0.04±1.45	2.83±4.12	27.89±3.45	32.16±2.56	0.89±2.89	-2.78±4.36
5	1.4	1.02±1.89	3.86±2.45	0.50±2.34	1.67±2.12	31.29±3.78	34.45±3.11	-4.56±4.74	-0.78±2.45
6	1.4	0.32±1.65	4.08±3.56	0.33±1.34	3.61±3.23	30.87±2.48	35.12±1.36	-7.08±5.65	-6.40±6.45
Mean ± SD		-0.89±1.61	3.37±1.35	0.08±0.31	1.85±1.17	29.86±1.63	33.08±0.90	-1.37±4.17	-2.93±2.58

Table 2.2 shows BOLD, TOLD responses, baseline transverse relaxation rates (air), and change in transverse relaxation rates in hypoxic regions and whole tumor of individual Dunning prostate R3327-AT1 tumors. In addition to the correlations obtained from change in R_2* with respect to BOLD, TOLD, HR/M, correlations between baseline (air) transverse relaxation rates and BOLD, TOLD, HR/M in hypoxic regions were observed to be 0.87, 0.82, 0.83 and corresponding p-values to be 0.002, 0.01, 0.03 respectively.

Table 2.3 [^{18}F] FMISO uptake in Hypoxic regions (HR), Whole tumor (WT), Muscle (M), Hypoxic region to muscle ratio (HR/M), Whole tumor to muscle ratio (WT/M) individual Dunning prostate R3327-AT1 tumors.

Rat	Size (cm^3)	HR(%ID/g)	WT(%ID/g)	M(%ID/g)	HR/M	WT/M
1	2.0	0.77±0.51	0.44±0.32	0.09±0.02	8.56	4.89
2	1.3	0.95±0.23	0.23±0.11	0.18±0.09	5.28	1.28
3	2.0	0.50±0.06	0.37±0.42	0.31±0.03	1.61	1.19
4	2.6	0.70±0.11	0.50±0.18	0.28±0.08	2.50	1.79
5	1.4	0.54±0.45	0.40±0.08	0.34±0.10	1.59	1.18
6	1.4	0.55±0.07	0.45±0.21	0.31±0.12	1.77	1.45
Mean ± SD		0.67±1.17	0.40±0.09	0.25±0.09	3.55±2.82	1 .96±1.45

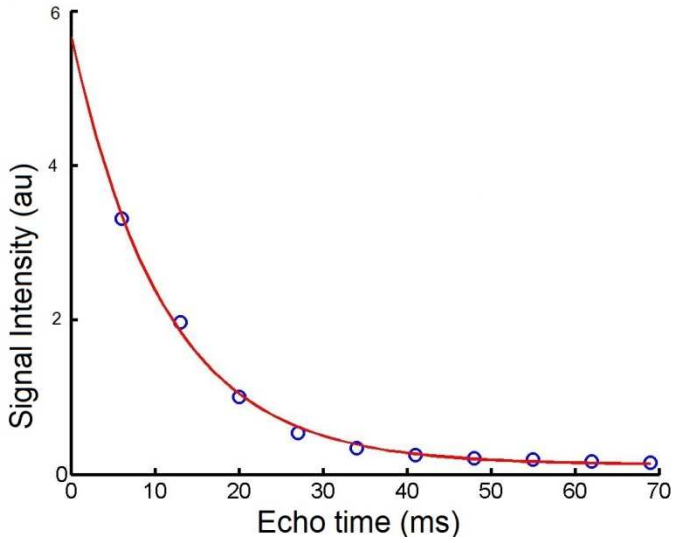

Figure 2.5 T_2* Decay curve of the tumor signal intensity as a function of echo time for Rat#2 for the whole tumor

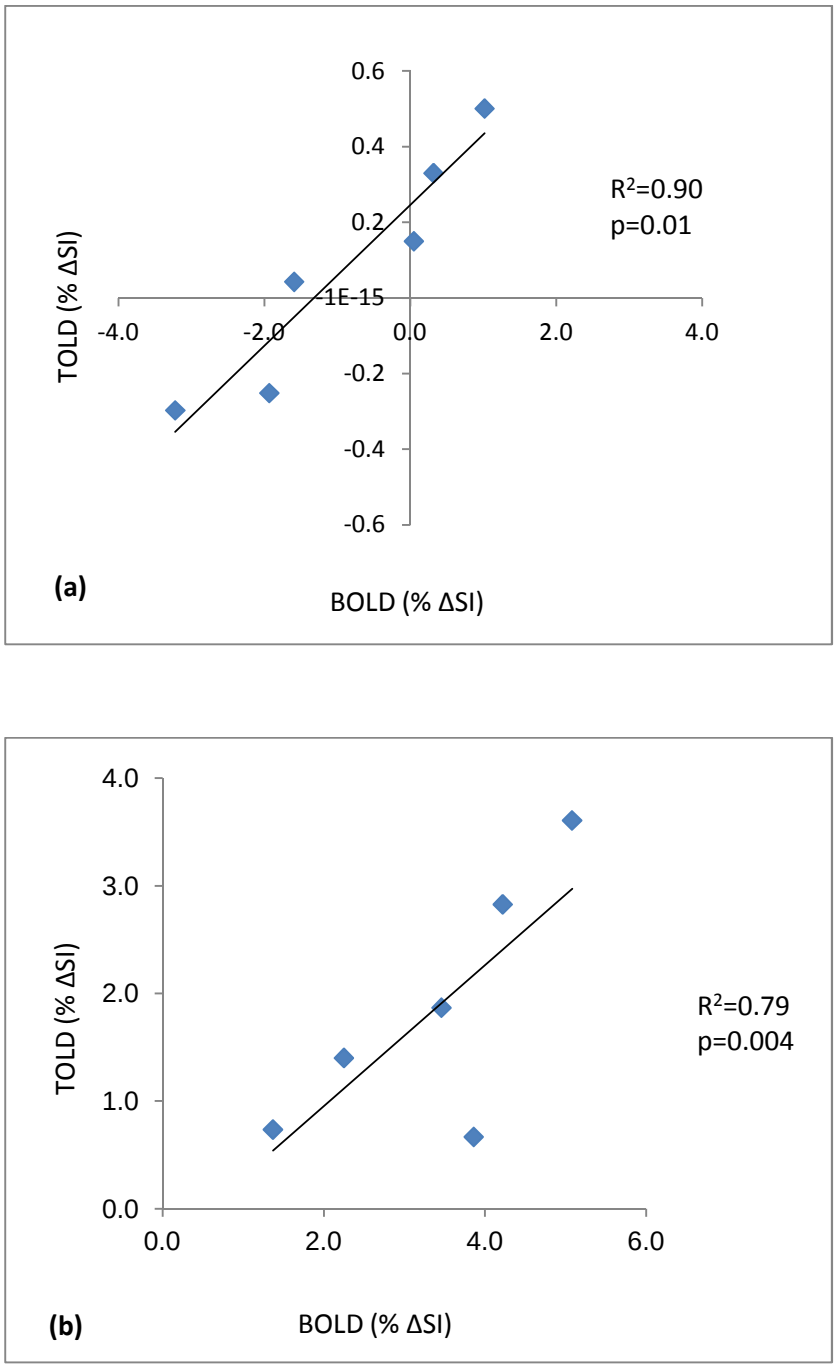

Figure 2.6 Correlations between BOLD and TOLD responses of individual tumors. (a)Hypoxic region and (b) Whole tumor.

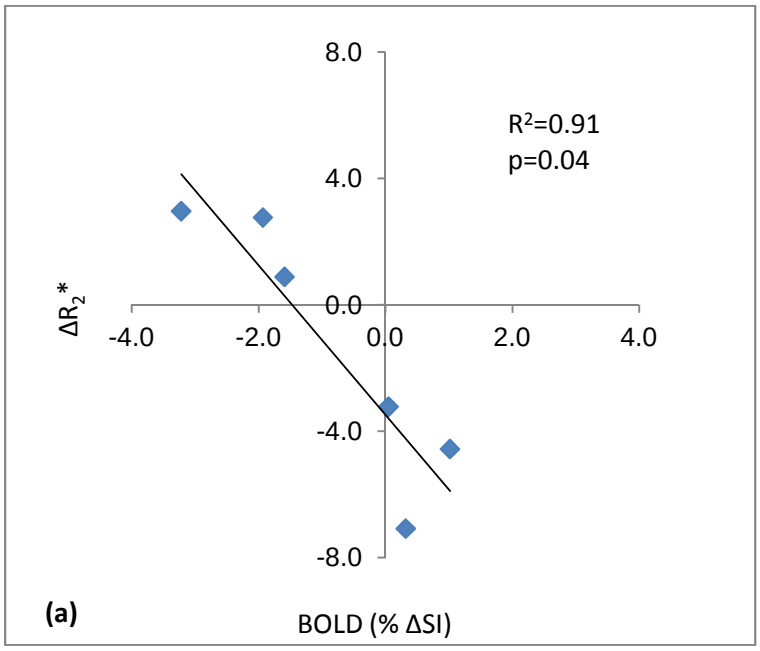

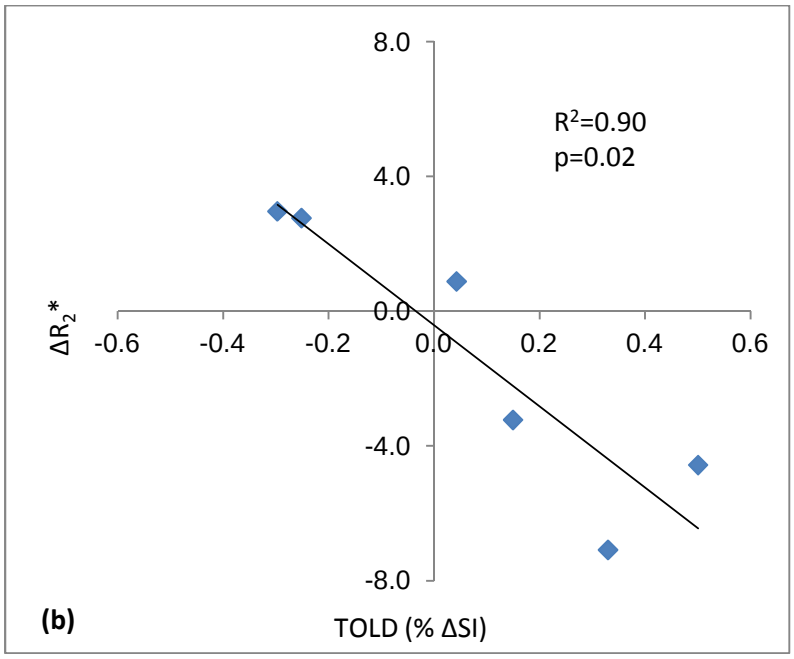

Figure 2.7 Correlations between BOLD and TOLD responses of individual tumors with ΔR_2^* in hypoxic regions. (a) BOLD response to ΔR_2^* (b) TOLD response to ΔR_2^*.

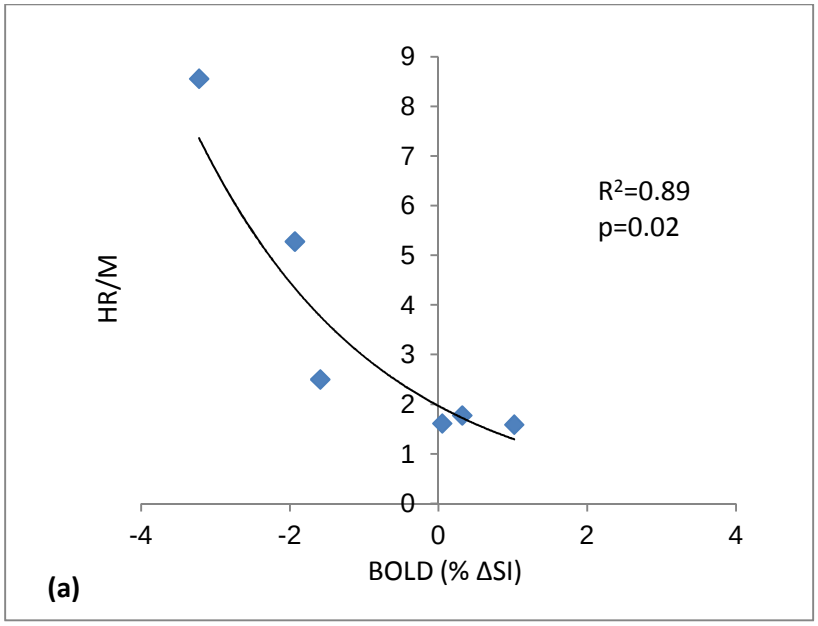

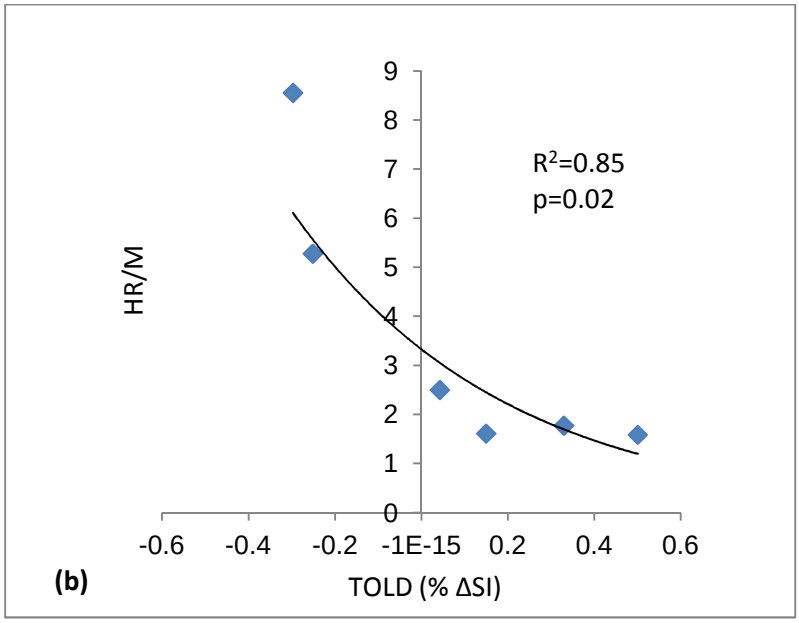

Figure 2.8 Correlations between BOLD and TOLD responses with Hypoxic region to muscle ratio (HR/M) of individual tumors. (a) Hypoxic region BOLD response to HR/M and (b) Hypoxic region TOLD response to HR/M.

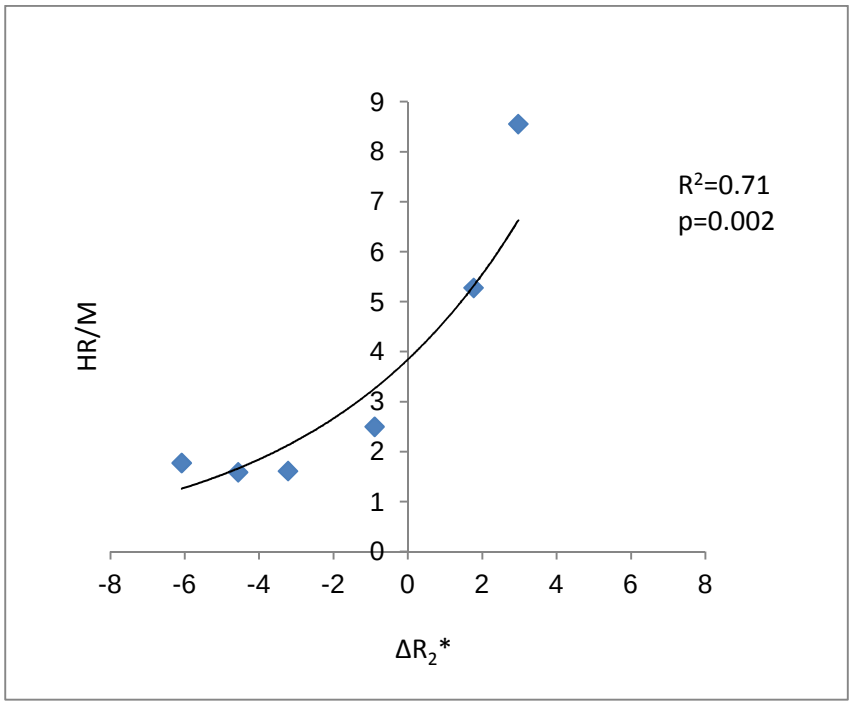

Figure 2.9 Correlation between ΔR_2*with Hypoxic region to muscle ratio (HR/M) of individual tumors in hypoxic region

2.4 Discussion

This study showed strong quantitative correlations between BOLD and TOLD responses of all tumors and these in turn correlated with the [^{18}F] FMISO uptake values using PET in corresponding ROIs. Also, R_2* values showed a robust correlation with [^{18}F] FMISO uptake in assessing hypoxic regions. However, individual tumors showed a wide range of hypoxic fractions in both MRI and PET.

The combination of BOLD and TOLD measurements is progressively more utilized for characterizing the tumors based on the regional response. [^{18}F] FMISO, a PET tracer regarded as hypoxic marker was used to see similar regional response to support the theory. The regions of high uptake of [^{18}F] FMISO corresponded to the lower BOLD and TOLD response regions on MRI provided an insight to separate the regions in the tumor and look at those regions more closely to characterize the tumors. My results provide additional substantiation for the utility of

oxygen-sensitive MRI for characterizing tumor hypoxia and separating the hypoxic regions from the tumor based on BOLD and TOLD responses in correlation with [^{18}F] FMISO PET results. Hence, this technique emerged as useful non-invasive technique to assess hypoxia, and discovered response to oxygen challenge. When applying these techniques to clinical studies, there are certain challenges that accounts to noise like respiratory or cardiac motion, motion due to swallowing, muscle contractions that occur in the digestive tract and bladder filling that may lead to signal subtraction.

Prominently, oxygen sensitive MRI reveals the spatial and temporal heterogeneity of oxygen dynamics and it is non-invasive, highly reproducible technique which is easy to implement. This appears to be the premier advantage of using oxygen sensitive MRI to assess tumor hypoxia.

2.5 Conclusion

The correlations between BOLD, TOLD and [^{18}F] FMISO uptake provide further impetus for the use of non-invasive oxygen sensitive MRI with respect to a oxygen challenge to evaluate tumor oxygenation emphasizing prospective value for translating it to clinical research. Tumor configuration based on the oxygen response (responsive and non-responsive regions) may allow therapy to be customized to treat the tumors. My results provide excellent impetus to further evaluate these techniques and apply in clinical research.

Acknowledgements

My study was supported by grants from the NIH NCI (R01 CA139043) and infrastructure provided by the Southwestern Small Animal Imaging Research Program (SW-SAIRP) supported by 1U24 CA126608. PET investigations were facilitated by the expert assistance of Dr. Srinivas Chiguru and Saleh Ramezani, MRI training by Dr. Rami Hallac and implantation of tumors by Marisela I. Aguilera and Joshua Gunpat.

CHAPTER 3

ASSESSING TUMOR HYPOXIA USING BOLD AND TOLD CONTRAST MRI IN SYNGENEIC DUNNING PROSTATE TUMORS

.

3.1 Abstract

This study examined the potential use of oxygen sensitive MRI to evaluate tumor response in various tumor sub-lines. BOLD and TOLD MRI which are oxygen sensitive were used to examine the oxygen response of subcutaneous tumors at 4.7T MRI system. Syngeneic Dunning R3327-H, -HI, -AT1, -MAT-Lu prostate tumors were implanted subcutaneously in male Copenhagen rats and were examined with respect to oxygen breathing challenge using interleaved BOLD (T_2*-weighted), which is sensitive to paramagnetic deoxyhemoglobin, and TOLD (T_1-weighted) sequence, sensitive to tumor tissue oxygenation. Strong correlations were observed between BOLD, TOLD and R_2* ($1/T_2$*) in response to oxygen challenge. Smaller responses were observed in more hypoxic tumors compared to less hypoxic tumors in terms of BOLD, TOLD and T_2* as discussed in Chapter 2. In this study, four different tumor sublines were examined which were in a wide range of tumor sizes providing a potential approach to observe the response of each tumor subline with respect to hypoxia. The observed correlations provide further impetus to use MRI ad a non-invasive technique to assess tumor hypoxia in response to oxygen challenge emphasizing impending value for clinical applications.

3.2 Introduction

Of various in vivo non-invasive techniques to assess tumor hypoxia, oxygen-sensitive MRI (BOLD and TOLD) is an attractive and reliable option. BOLD and TOLD contrast MRI in patients is being increasingly used [16, 19, 20, 24, 43, 45, 56-58]. BOLD MRI is based on tumor

blood oxygenation and its response to hyperoxic gas breathing serves as a non-invasive indicator of hypoxia and it is also sensitive to pH, bold flow, vascular volume and vessel density[16, 20]. TOLD MRI is based on T_1-weighted contrast and is sensitive to tissue oxygenation [28, 59, 60]. In this study, I investigated the potential use of BOLD and TOLD in four different tumor sublines and their response to oxygen challenge based on T_1 , T_2* weighted images and transverse relaxation rates (R_2*) to assess tumor oxygenation.

These four different tumor sublines namely Dunning R3327-H, -HI, -AT1 or –MAT-Lu have different characteristics based on metastasis, growth, differentiation. Also, tumors of various sizes were taken and examined to see how these different sublines respond to oxygen challenge [61-65]. Diverse patterns of hypoxia and oxygenation were observed in this study. Here, I examined BOLD and TOLD MRI as alternative biomarkers to assess tumor oxygenation.

3.3 Materials and Methods

3.3.1 Animal Model

This study was approved by the Institutional Animal Care and Use Committee. Twelve male Copenhagen rats were implanted subcutaneously with Dunning R3327-H, -HI, -AT1 or –MAT-Lu tumors. A small incision is made in the thigh portion of the rat and the tumor tissue fragments were surgically implanted subcutaneously. H is a well-differentiated, low metastatic, slow growing tumor subline with a tumor volume doubling time of 21 days. HI is a non-metastatic, hormone insensitive, moderately differentiated, slow growing subline. The tumor volume doubling time of HI is 9 days. AT1 is an anaplastic, low metastatic, comparatively fast growing tumor subline with tumor volume doubling time of 5.2 days. MAT-Lu is an anaplastic, high metastatic, fast growing tumor subline with tumor volume doubling time of 2.7 days. Tumor volume was calculated as V= (π/6)*a*b*c, where a, b, c, are the three orthogonal diameters of the tumor. For MRI, the rats were maintained under general gaseous anesthesia (1.3% isoflurane in air (1L/min); Baxter International, Deerfield, IL).

3.3.2 Tumor oximetry

Twelve rats bearing SC Dunning prostate Dunning R3327-H, -HI, -AT1 or –MAT-Lu tumors were examined with respect to oxygen breathing challenge using interleaved BOLD (T_2* weighted) contrast, which is sensitive to paramagnetic de-oxyhemoglobin and TOLD (T_1 weighted) sensitive to tumor tissue oxygenation (pO_2). High resolution T_2-weighted anatomical images were acquired using Fast spin echo sequence (TR=2000 ms, effective TE=48 ms, Echo Train Length (ETL) = 8, 128X128 data matrix, 40X40 mm FOV, 1 mm slice thickness without gap). Interleaved BOLD and TOLD sequence (IBT) with baseline (air) followed by oxygen challenge was run. BOLD used Multi-echo Gradient Echo (TR=150 ms, 10 echo times TE=6-69 ms with echo spacing of 7 ms, flip angle (FA) = 20°, acquisition time 21 s. 128X128 data matrix, 40X40mm FOV) and TOLD uses Gradient Echo sequence (TR=30ms, TE=5ms, flip angle (FA) = 45°, acquisition time 3 seconds, 128X128 data mat rix, 40X40 mm FOV).

3.3.3 Results

In this study, twelve Copenhagen rats were investigated (3 H, 3 HI, 3 AT1 and 3 MAT-Lu). IBT studies were performed with oxygen challenge and SI (%ΔSI) for BOLD, TOLD, ΔR_2*were calculated. While breathing air, all measurements were found to be stable. Upon oxygen breathing, a change in BOLD (%ΔSI), TOLD (%ΔSI) and ΔR_2* were observed in all tumor sublines. When all tumors are considered, an average change in BOLD ΔSI = 4.44±3.35%, TOLD ΔSI =1.58±1.52%, and transverse relaxation rate (ΔR_2*) = -1.64±1.75 were observed.

Dunning R3327-H tumor which is considered as well-differentiated, low metastatic, slow growing tumor subline showed an average BOLD ΔSI = 5.79±4.76%, TOLD ΔSI =2.12±1.67%, and transverse relaxation rate (ΔR_2*) = -1.92±1.22. Dunning R3327-HI tumor which is a non-metastatic, hormone sensitive, moderately differentiated, slow growing subline showed an average BOLD ΔSI = 4.23±3.79%, TOLD ΔSI =1.55±1.86%, and transverse relaxation rate

(ΔR_2*) = -2.07±2.23. Dunning R3327-AT1 tumor which is an anaplastic, low metastatic, comparatively fast growing tumor subline showed an average BOLD ΔSI = 4.09±2.66%, TOLD ΔSI =0.97±1.46%, and transverse relaxation rate (ΔR_2*) = -1.14±0.78. Dunning R3327-MAT-Lu tumor which is an anaplastic, high metastatic, fast growing tumor subline showed an average BOLD ΔSI = 3.66±3.72%, TOLD ΔSI =1.67±1.85%, and transverse relaxation rate (ΔR_2*) = -1.44±3.01. All the tumors were in a wide range of tumor sizes. It was observed that small tumors showed a higher response to oxygen than the large tumors in terms of BOLD and TOLD.

Strong correlations were observed in terms of mean changes in BOLD, TOLD and R_2*. Student t-test was used to find the p-value. The p-value for BOLD and TOLD was observed to be 0.004(R^2=0.87), BOLD and ΔR_2* was observed to be 0.02 (R^2=0.83) and TOLD and ΔR_2* was observed to be 0.006 (R^2=0.81). The results are said to be significant as the p-values are less than 0.05.

Baseline (air) transverse relaxation rates (R_2*) were added to the data to see if there is any correlation between baseline R_2* with respect to BOLD and TOLD. The correlation parameters of R_2* Vs BOLD, R_2* Vs TOLD were observed to be R^2=0.87 (p=0.01) and 0.83 (p=0.03) respectively.

Also, data obtained from Chapter 2 of AT1 tumors was added to the data of Chapter 3 (n=18) to see if the correlation parameters are consistent. R^2 values of BOLD Vs TOLD, BOLD Vs ΔR_2*, TOLD Vs ΔR_2*, BOLD Vs Tumor size, TOLD Vs Tumor size, ΔR_2* Vs tumor size were observed to be 0.78, 0.72, 0.58, 0.73, 0.65, 0.63 respectively. The data obtained for Rat#3 of AT1 tumor appeared to be an outlier (more hypoxic) in most of the cases and when ignored, the R^2 values were observed to be 0.84, 0.79, 0.72, 0.78, 0.69, and 0.68 respectively.

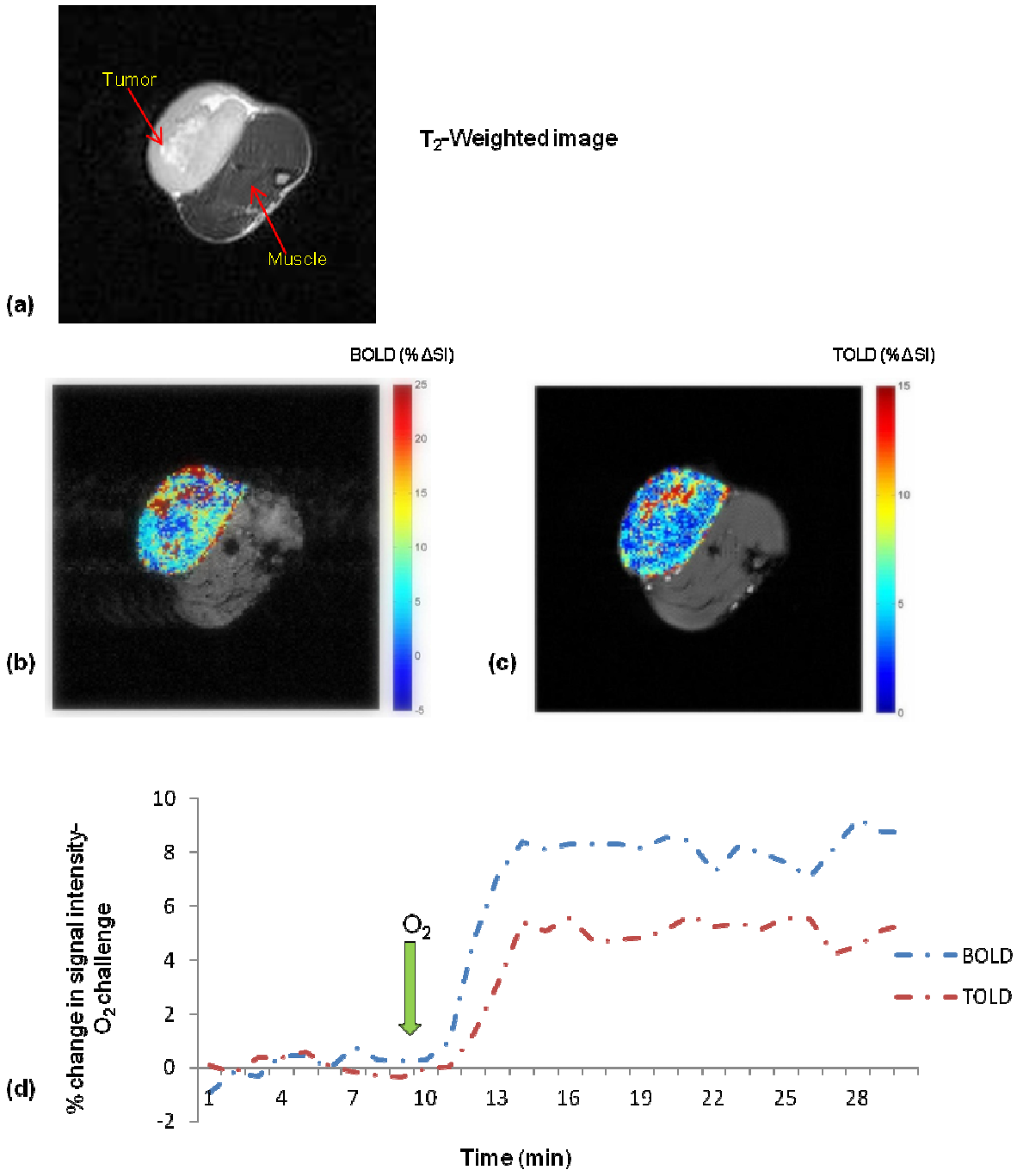

Figure 3.1 Oxygen sensitive MRI of Rat#1-MAT-Lu. (a) High resolution T_2-W image showing the tumor and muscle, (b) BOLD, (c) TOLD, (d) Changes in tumor oxygenation in response to oxygen breathing: mean changes in BOLD (blue) and TOLD (red).

Table 3.1 Effect of oxygen breathing on BOLD and TOLD MRI and R_2* of Dunning prostate R3327-H, -HI, -AT1 and –MAT-Lu tumors.

Tumor type	Rat #	Size (cm^3)	BOLD (%ΔSI)	TOLD (%ΔSI)	Baseline R_2* (s^{-1})- air	ΔR_2* (s^{-1})
H	1	2.2	2.00±2.45	1.54±0.43	32.97±1.43	-0.8±0.22
	2	0.5	11.14±3.65	4.01±1.12	47.87±1.45	-3.23±1.23
	3	0.9	4.23±1.09	0.81±0.65	43.56±0.34	-1.73±0.54
HI	1	1.8	3.22±0.78	0.09±0.05	38.56±0.54	-2.22±0.23
	2	0.6	8.43±1.56	3.65±0.89	42.22±0.67	-4.24±1.34
	3	1.4	1.05±1.01	0.91±1.23	36.12±1.34	0.23±0.11
AT1	1	1.9	1.04±0.23	0.04±1.02	32.56±1.54	-1.22±0.26
	2	0.7	5.94±1.40	2.66±1.23	42.87±2.12	-1.89±0.89
	3	0.5	5.3±2.67	0.23±0.78	35.87±1.78	-0.33±1.11
MAT-Lu	1	0.5	7.57±2.12	3.72±1.22	45.99±1.65	-4.56±2.34
	2	2.4	0.16±0.08	0.09±0.67	36.09±0.98	1.45±0.98
	3	1.2	3.27±0.98	1.22±0.87	36.78±0.67	-1.23±0.34

Table 3.1 shows the BOLD, TOLD changes and mean ΔR_2* values in response to oxygen challenge for each tumor subline along with the tumor volumes. The respective correlation plots are shown in figures 2-2, 2-3, and 2-4.

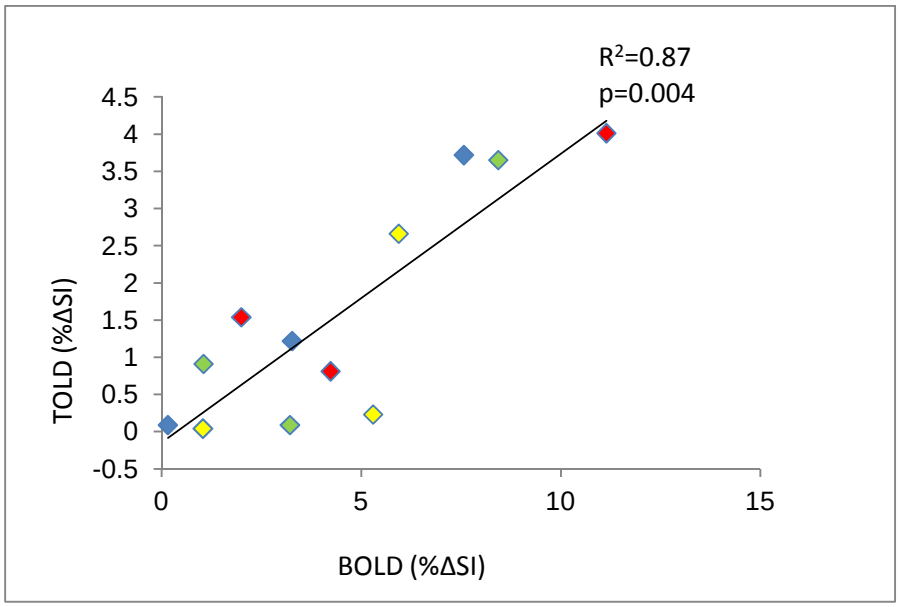

Figure 3.2 Comparison of BOLD and TOLD response to oxygen challenge for H (red), HI (green), AT1 (yellow) and MAT-Lu (blue) tumors. Correlation of BOLD and TOLD based on mean change in signal intensity due to oxygen breathing.

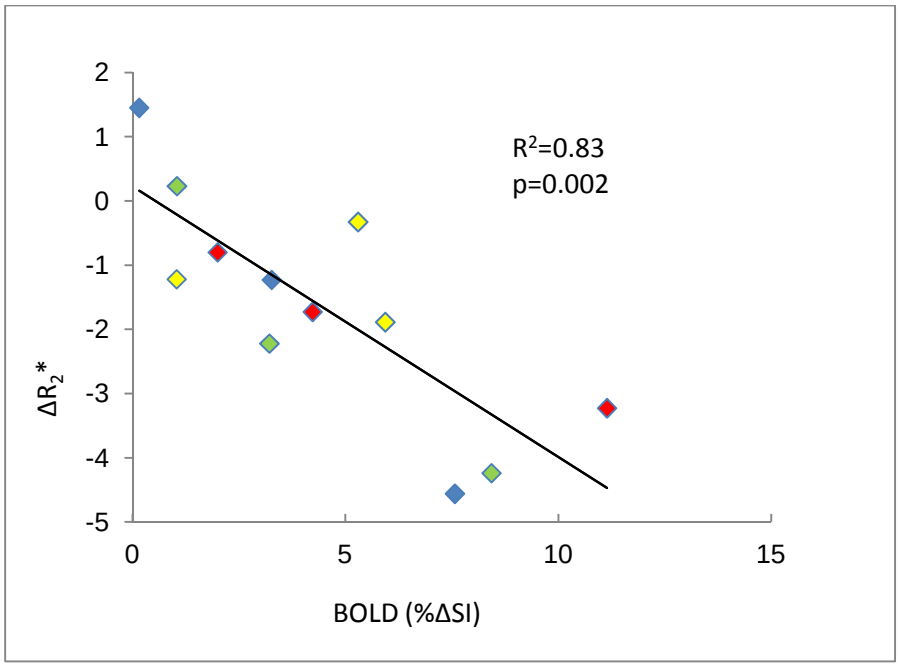

Figure 3.3 Comparison of BOLD response and mean change in transverse relaxation rates to oxygen challenge for H (red), HI (green), AT1 (yellow) and MAT-Lu (blue) tumors. Correlation of average change in BOLD and R_2* due to oxygen breathing.

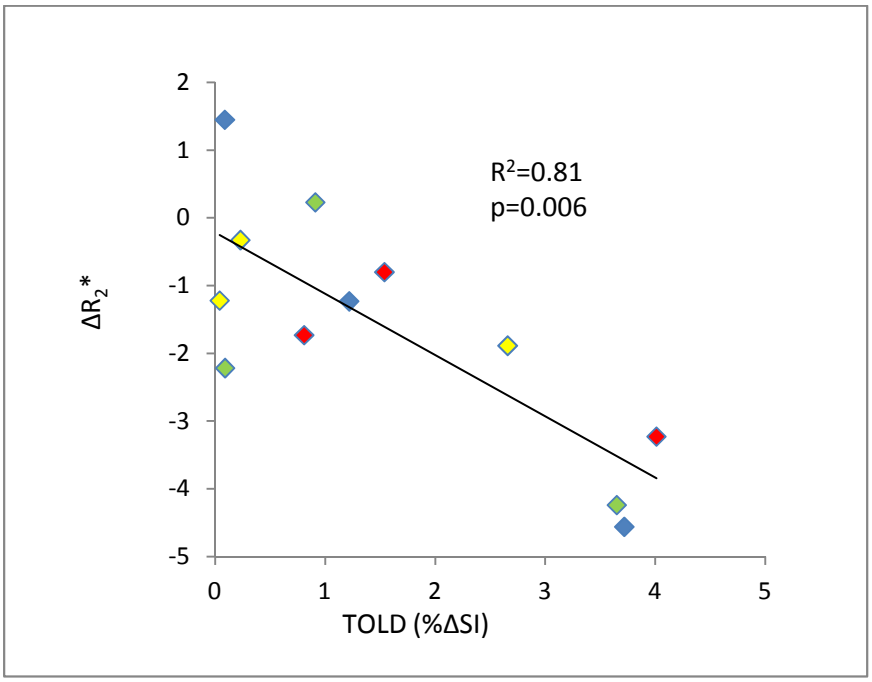

Figure 3.4 Comparison of TOLD response and mean change in transverse relaxation rates to oxygen challenge for H (red), HI (green), AT1 (yellow) and MAT-Lu (blue) tumors. Correlation of average change in TOLD and R_2* due to oxygen breathing.

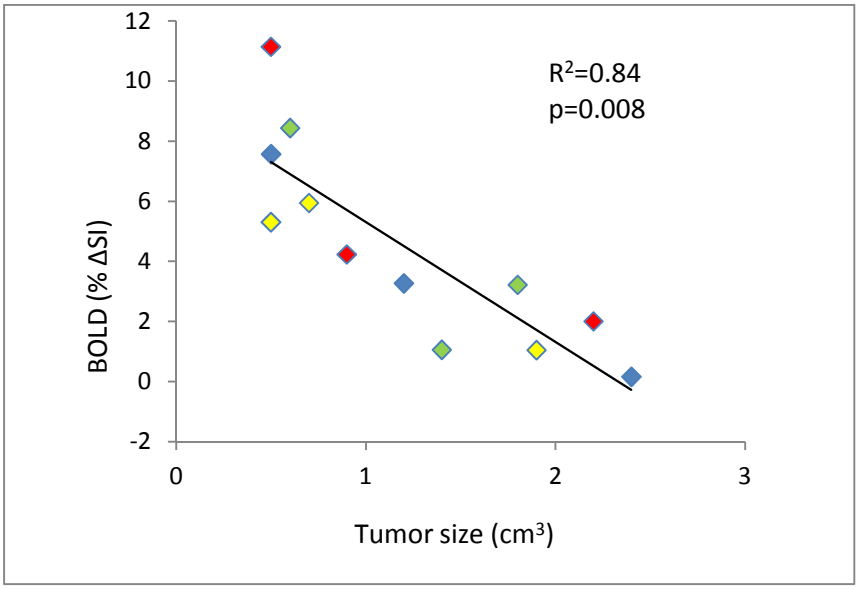

Figure 3.5 Comparison of BOLD responses (% ΔSI) of H (red), HI (green), AT1 (yellow) and MAT-Lu (blue) tumors to tumor size (cm^3)

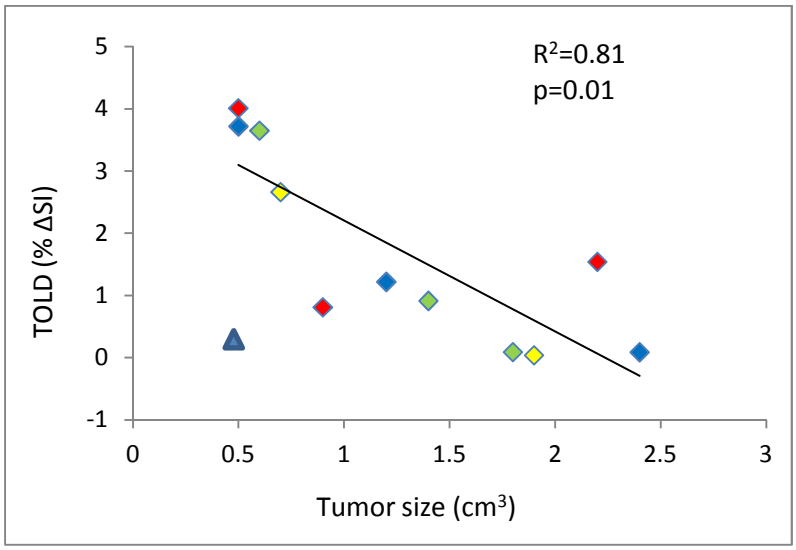

Figure 3.6 Comparison of TOLD response (% ΔSI) of H (red), HI (green), AT1 (yellow) and MAT-Lu (blue) tumors to tumor size (cm^3). (Outlier denoted in different symbol)

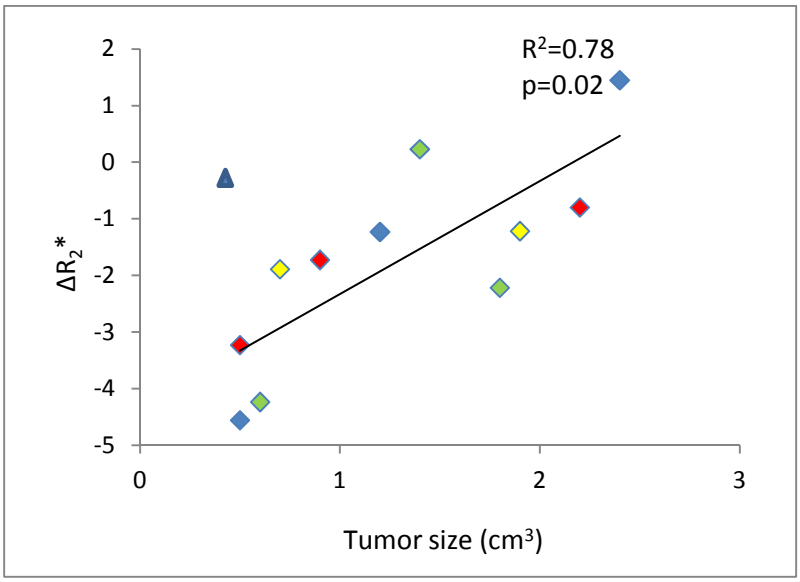

Figure 3.7 Comparison of mean change in transverse relaxation rate (ΔR_2^*) of H (red), HI (green), AT1 (yellow) and MAT-Lu (blue) tumors to tumor size (cm^3). (Outlier denoted in different symbol)

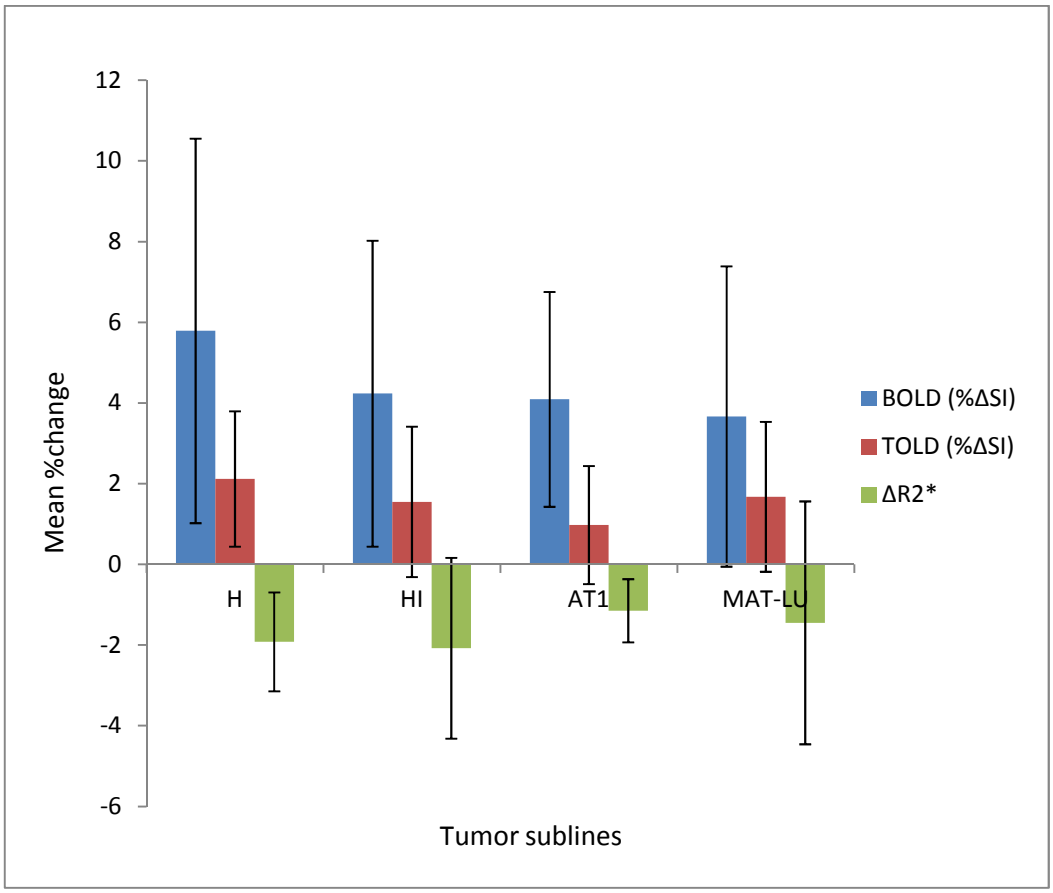

Figure 3.8 Bar graph comparing BOLD, TOLD responses and R_2* in R3327-H, -HI, -AT1 and –MAT-Lu tumors. Mean changes in BOLD, TOLD responses and R_2* with standard deviation as error bars in individual sublines. Change in signal intensity of BOLD ($\%\Delta SI$) in blue, TOLD ($\%\Delta SI$) in red and mean changes in R_2* (ΔR_2*) in green.

3.4 Discussion

This study showed strong correlations between BOLD and TOLD responses and gave consistent results. The small tumors (tumor size <1cm^3) showed a higher BOLD and TOLD response to oxygen compared to the large ones when the results of all tumor sublines that are Dunning R3327-H, -HI, -AT1 or –MAT-Lu are combined. This suggests that the smaller tumors are well oxygenated; whereas the larger ones (tumor size > 2cm^3) are hypoxic, although when individual tumors are considered, they showed heterogeneity. Smaller tumors exhibited larger

changes in BOLD ((%ΔSI = 7.1±2.49%), TOLD ((%ΔSI = 2.51±1.64%) and larger tumors exhibited smaller changes in BOLD ((%ΔSI =1.03±1.3%), TOLD ((%ΔSI = 0.5±1.04%) showing that the smaller tumors are comparatively well oxygenated [62-65].

Strong correlations were found in terms of quantitative BOLD, TOLD responses and ΔR_2^* (R^2>0.8). Combining BOLD and TOLD measurements is gradually more utilized for characterizing normal tissues and tumors in patients. The differences in BOLD and TOLD response in different tumor lines did not reach statistical significance for the groups and it could be understood better when a large group of rats are considered for the study. The difference in oxygenation and hypoxia was observed based on the tumor volume rather than the tumor subline as n=3 in each group. Though there are four different tumor sublines (R3327-H, -HI, -AT1 or –MAT-Lu) in the combined group, they showed strong correlations in BOLD and TOLD with respect to oxygen challenge.

My results provide further confirmation for the efficacy of oxygen-sensitive MRI for characterizing tumor hypoxia. The T_2^*-weighted measurements correspond with independent BOLD and TOLD responses to oxygen breathing for these tumors [66]. This appears to be the foremost advantage of using oxygen sensitive MRI to assess tumor hypoxia.

3.5 Conclusion

These results provide a potential insight into the associations between oxygen sensitive MRI (BOLD and TOLD) parameters in response to oxygen challenge. The response of various tumor sublines Dunning R3327-H, -HI, -AT1 or –MAT-Lu to oxygen breathing were studied using oxygen sensitive MRI focusing on pre-clinical models of prostate cancer in Copenhagen rats. The results provide motivation for expanding the studies to other tumor sites. As the method is exclusively non-invasive, highly reproducible and easy to implement, further application of these techniques in clinical research is important.

CHAPTER 4

PRELIMINARY STUDIES OF BOLD AND TOLD CONTRAST MRI IN PC3 ORTHOTOPIC PROSTATE TUMORS

4.1 Introduction

In the previous chapters of preclinical investigations, I demonstrated the efficacy of BOLD and TOLD contrast MRI in Dunning prostate R2237 tumor models implanted subcutaneously in Copenhagen rats. In this chapter, I will discuss the potential use of BOLD and TOLD contrast MRI in Orthotopic prostate tumor model. The orthotopic tumor models present a degree of complexity superior to traditional subcutaneous tumor models. In order to establish an appropriate tumor microenvironment that allows for the emergence of metastatic phenotype, phenotypic divergence of tumor heterogeneity, there is a necessity of importance of orthotopic tumor implantation[67-71]. Study of orthotopic tumor models remains as the stronghold of related biology for the study of therapeutic strategies and explanation of molecular events associated with progression, metastasis and therapy of cancer [72]. Orthotopic tumor models are more appropriate to study as they are more close to clinical models and provide a potential insight to be translated to clinical research.

In this study, orthotopic prostate tumors were examined using oxygen sensitive MRI (BOLD and TOLD) with respect to oxygen challenge and Dynamic Contrast Enhancement MRI as a validation [73, 74]. The tumor response to oxygen breathing is examined using BOLD and TOLD contrast MRI.

4.2 Materials and Methods

4.2.1 Animal model

This study was approved by the Institutional Animal Care and Use Committee. Tumors were propagated by injecting 2.5 million PC3 –luc cells orthotopically into the prostate gland of male nude rats. The PC3 cells were luciferase transfected before implantation to study the growth of the tumor using Bioluminescence Imaging. Also, weekly ultrasound imaging is done to monitor the tumor growth. Once tumors reached a palpable mass, MRI was performed.

4.2.2 Tumor oximetry

Two rats with orthotopic tumors implanted using PC3 cells were examined using Litzcage volume coil module (60 mm diameter x 60 mm rung length, $^{1}H/^{19}F$ dual frequency – Doty scientific) at 4.7T Animals were anesthetized with isoflurane (1.3%) in air (1 L/min) and kept warm (37 ℃) using a circulating warm water bl anket.

Tumors were examined with respect to oxygen breathing challenge using interleaved BOLD (T_2* weighted) contrast, which is sensitive to paramagnetic de-oxyhemoglobin and TOLD (T_1 weighted) sensitive to tumor tissue oxygenation (pO_2). High resolution T_2-weighted anatomical images were acquired using Fast spin echo sequence (TR=2000 ms, effective TE=48 ms, Echo Train Length (ETL) = 8, 128X128 data matrix, 60X60 mm FOV, 2 mm slice thickness without gap). Interleaved BOLD and TOLD sequence (IBT) with baseline (air) followed by oxygen challenge was run. BOLD used Multi-echo Gradient Echo (TR=150 ms, 10 echo times TE=6-69 ms with echo spacing of 7 ms, flip angle (FA) = 20°, 128X128 data matrix, 40X40mm FOV) and TOLD uses Gradient Echo sequence (TR=30 ms, TE=5 ms, flip angle (FA) = 45°, 128X128 data matrix, 60X60 mm FOV).

4.2.3 Dynamic Contrast Enhanced MRI

Following IBT, time course DCE data were acquired continuously using a Gradient Echo sequence (TR=40 ms, TE=2.58 ms, flip angle (FA) = 45°, 128X128 data matrix, 60X60 mm FOV) post-injection of 0.1 mmole/kg body weight Gd-DTPA (Gadavist®) intravenously. Spatial resolution of DCE Images is kept same as BOLD/TOLD. 60 dynamic images and acquisition time of each dynamic is 10 sec

4.2.4 Results

I investigated two tumors using oxygen sensitive MRI in response to oxygen challenge. The two tumors behaved similarly in terms of baseline measurements using air. When the gas was switched to oxygen, similar to the subcutaneous tumors, there was an increase in signal intensity of both BOLD and TOLD.

For rat 1, average change in BOLD ΔSI = 5.4±2.2%, TOLD ΔSI =2.8±1.5%, and ΔR_2^*= -2.4±2.9 were observed. The respective images and dynamic plots are shown in Figure 4-1. Also, DCE curves are plotted for tumor and muscle which is shown in Figure 4-2.

For rat 2, average change in BOLD ΔSI = 3.4±2.6%, TOLD ΔSI =1.8±1.9%, and ΔR_2^*= -1.4±2.2 were observed.

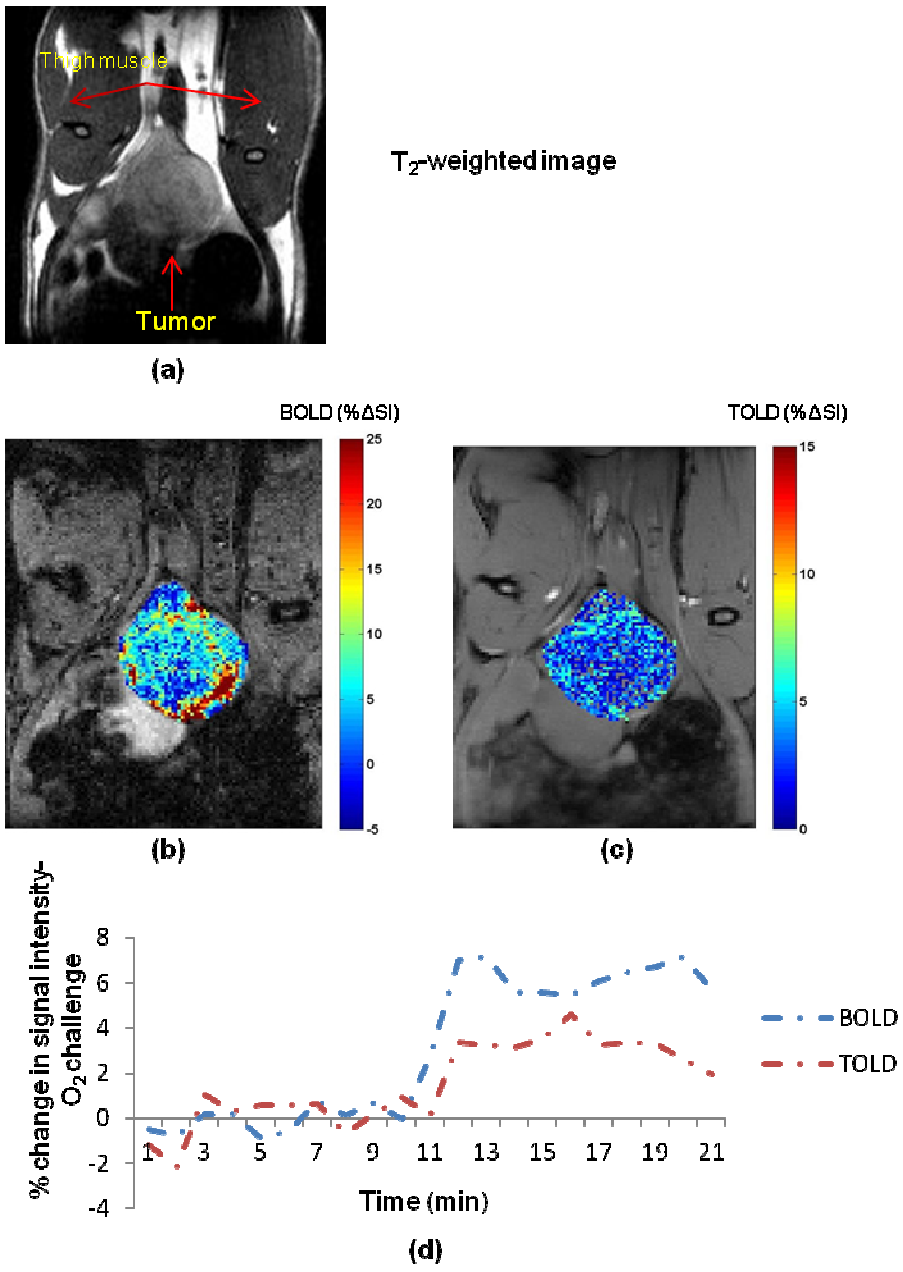

Figure 4.1 Oxygen sensitive MRI OF Rat #1. (a) High resolution T_2-W image showing the tumor and muscle, (b) BOLD, (c) TOLD, (d) Changes in tumor oxygenation in response to oxygen breathing: mean changes in BOLD (blue) and TOLD (red).

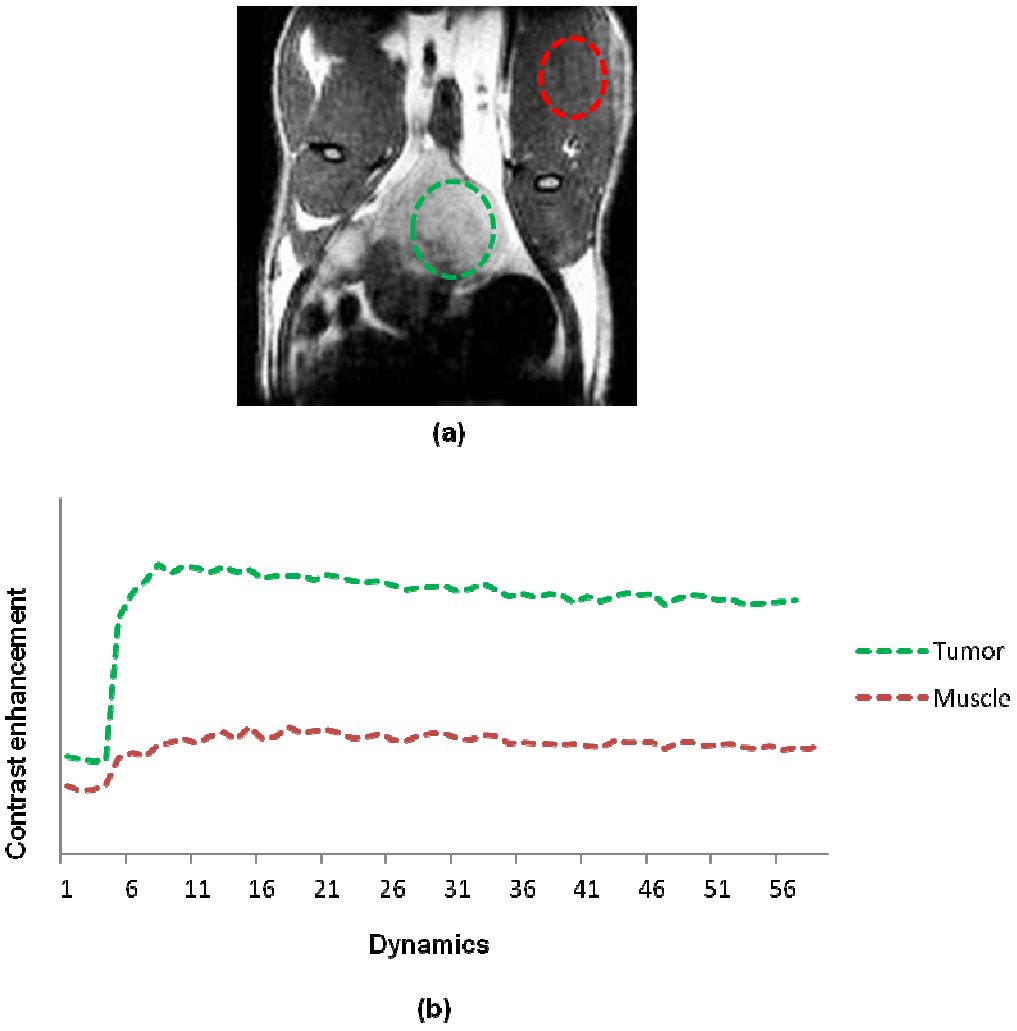

Figure 4.2 Dynamic contrast enhanced MRI. (a) High resolution T_2-W image showing the tumor (green) and muscle (red), (b) Contrast enhancement plot for 60 dynamic images.

4.3 Discussion

From the results obtained by investigating two rats with orthotopic prostate tumor, it is evident that the BOLD and TOLD responses of these tumors are similar to the responses obtained in subcutaneous tumors. However, there are a few challenges while investigating the orthotopic tumors such as low signal to noise ratio, motion of the organs inside the body. To increase signal to noise ratio, acquisition time could be increased however, it affects the signal as there would be motion artifacts which could be eliminated by decreasing the acquisition time. Hence, an optimal acquisition time is required to image orthotopic tumors. If such complications are eliminated, oxygen sensitive MRI is feasible in clinical research.

4.4 Conclusion and future directions

In Chapter 2, variation in BOLD and TOLD signal responses observed in syngeneic Dunning R3327-AT1 prostate tumor, with respect to oxygen breathing were compared with [^{18}F]-Fluoromisonidazole (^{18}FMISO) PET in hypoxic regions. Significant correlations were found between oxygen sensitive (BOLD and TOLD) MRI and [^{18}F] FMISO PET measurements for oxygen breathing for whole tumor measurements as well as for hypoxic regions.

In addition, variation in BOLD and TOLD signal response in syngeneic Dunning R3327-H, -HI, -AT1, -MAT-Lu prostate tumor sublines with respect to oxygen breathing was examined. In addition, the dependence of BOLD and TOLD signal response on tumor size is investigated. Considerable correlations were found between BOLD and TOLD MRI and tumor size. It was observed from my study that the larger tumors showed smaller BOLD and TOLD response than the smaller tumors. When the MRI results of Chapter 2 were added to Chapter 3, the results were observed to be consistent. From the data I acquired, it was observed that the BOLD and

TOLD response is more dependent on tumor size rather than the tumor subline. To investigate the BOLD/TOLD dependence of tumor sublines, the study needs more animals to be examined which provides a better vision on the dependence based on the tumor subline. Previous studies by Rami Hallac from our lab also showed lower BOLD and TOLD responses of large tumors compared to small tumors.

The orthotopic tumor models present a degree of complexity superior to traditional subcutaneous tumor models. As tumor microenvironment plays a major role in tumor progression, future preclinical studies should focus on evaluating BOLD, TOLD and DCE on orthotopic tumors. Preliminary studies on orthotopic PC3 tumors were done to examine the efficacy of BOLD and TOLD contrast MRI to assess tumor hypoxia. They yielded convincing results providing a potential approach to translate BOLD and TOLD contrast MRI for clinical translation. Also, performing the experiments during tumor growth provides important information of tumor oxygenation. Orthotopic tumor models are more suitable to study as they are more close to clinical models and provide a potential insight to be translated to clinical research. The limited results in Chapter 4 indicate proof of principle for future studies.

REFERENCES

1. Swartz, M.A., et al., *Tumor microenvironment complexity: emerging roles in cancer therapy*: Cancer Res. 2012 May 15;72(10):2473-80. doi: 10.1158/0008-5472.CAN-12-0122. Epub 2012 Mar 13.
2. Hockel, M. and P. Vaupel, *Tumor hypoxia: definitions and current clinical, biologic, and molecular aspects.* J Natl Cancer Inst, 2001. **93**(4): p. 266-76.
3. Vaupel, P. and L. Harrison, *Tumor hypoxia: causative factors, compensatory mechanisms, and cellular response.* Oncologist, 2004. **5**: p. 4-9.
4. Vaupel, P., O. Thews, and M. Hoeckel, *Treatment resistance of solid tumors: role of hypoxia and anemia.* Med Oncol, 2001. **18**(4): p. 243-59.
5. Folkman, J., *The vascularization of tumors.* Sci Am, 1976. **234**(5): p. 58-64.
6. Konerding, M.A., et al., *Evidence for characteristic vascular patterns in solid tumours: quantitative studies using corrosion casts.* Br J Cancer, 1999. **80**(5-6): p. 724-32.
7. Vaupel, P., D.K. Kelleher, and M. Höckel, *Oxygenation status of malignant tumors: Pathogenesis of hypoxia and significance for tumor therapy.* Seminars in Oncology, 2001. **28, Supplement 8**(0): p. 29-35.
8. Davda, S. and T. Bezabeh, *Advances in methods for assessing tumor hypoxia in vivo: Implications for treatment planning.* Cancer and Metastasis Reviews, 2006. **25**(3): p. 469-480.
9. Mason, R.P., et al., *Multimodality imaging of hypoxia in preclinical settings.* Q J Nucl Med Mol Imaging, 2010. **54**(3): p. 259-80.
10. Leach, M.O., et al., *The design and use of a dual-frequency surface coil providing proton images for improved localization in [sup 31]P spectroscopy of small lesions.* Medical Physics, 1986. **13**(4): p. 510-513.
11. Weishaupt, D., V. Kochli, and B. Marincek, How Does Mri Work?: An Introduction to the Physics And Function of Magnetic Resonance Imaging. 2006: Springer.
12. Prasad, P.V., R.R. Edelman, and F.H. Epstein, *Noninvasive Evaluation of Intrarenal Oxygenation With BOLD MRI.* Circulation, 1996. **94**(12): p. 3271-3275.
13. Liu, H., et al., *Noninvasive Investigation of Blood Oxygenation Dynamics of Tumors by Near-Infrared Spectroscopy.* Appl. Opt., 2000. **39**(28): p. 5231-5243.
14. Kuperman, V., et al., *Changes in T2*-weighted images during hyperoxia differentiate tumors from normal tissue.* Magn Reson Med, 1995. **33**(3): p. 318-25.
15. Robinson, S.P., F.A. Howe, and J.R. Griffiths, *Noninvasive monitoring of carbogen-induced changes in tumor blood flow and oxygenation by functional magnetic resonance imaging.* Int J Radiat Oncol Biol Phys, 1995. **33**(4): p. 855-9.
16. Howe, F.A., et al., *Issues in flow and oxygenation dependent contrast (FLOOD) imaging of tumours.* NMR Biomed, 2001. **14**(7-8): p. 497-506.
17. Robinson, S.P., et al., *Tumor vascular architecture and function evaluated by non-invasive susceptibility MRI methods and immunohistochemistry.* J Magn Reson Imaging, 2003. **17**(4): p. 445-54.
18. Fernández-Seara, M.A. and F.W. Wehrli, *Postprocessing technique to correct for background gradients in image-based R*(2) measurements.* Magnetic Resonance in Medicine: Official Journal of the Society of Magnetic Resonance in Medicine / Society of Magnetic Resonance in Medicine, 2000. **44**(3): p. 358-66.
19. Padhani, A., *Science to practice: what does MR oxygenation imaging tell us about human breast cancer hypoxia?* Radiology, 2010. **254**(1): p. 1-3.

20. Baudelet, C. and B. Gallez, *Current Issues in the Utility of Blood Oxygen Level Dependent MRI for the Assessment of Modulations in Tumor Oxygenation.* Current Medical Imaging Reviews, 2005. **1**(3): p. 229-243.
21. Neeman, M., et al., *In vivo BOLD contrast MRI mapping of subcutaneous vascular function and maturation: validation by intravital microscopy.* Magn Reson Med, 2001. **45**(5): p. 887-98.
22. Zhao, D., et al., *Comparison of 1H blood oxygen level-dependent (BOLD) and 19F MRI to investigate tumor oxygenation.* Magn Reson Med, 2009. **62**(2): p. 357-64.
23. Al-Hallaq, H.A., et al., *Spectrally inhomogeneous BOLD contrast changes detected in rodent tumors with high spectral and spatial resolution MRI.* NMR Biomed, 2002. **15**(1): p. 28-36.
24. Hallac, R.R., et al., *Oxygenation in cervical cancer and normal uterine cervix assessed using blood oxygenation level-dependent (BOLD) MRI at 3T.* NMR Biomed, 2012. **25**(12): p. 1321-30.
25. Jiang, L., et al., *Comparison of BOLD contrast and Gd-DTPA dynamic contrast-enhanced imaging in rat prostate tumor.* Magn Reson Med, 2004. **51**(5): p. 953-60.
26. Jiang, L., et al., *Blood oxygenation level-dependent (BOLD) contrast magnetic resonance imaging (MRI) for prediction of breast cancer chemotherapy response: A pilot study.* J Magn Reson Imaging, 2012. **2**(10): p. 23891.
27. Howe, F.A., et al., *Flow and oxygenation dependent (FLOOD) contrast MR imaging to monitor the response of rat tumors to carbogen breathing.* Magn Reson Imaging, 1999. **17**(9): p. 1307-18.
28. O'Connor, J.P., et al., *Comparison of normal tissue R1 and R*2 modulation by oxygen and carbogen.* Magn Reson Med, 2009. **61**(1): p. 75-83.
29. Burrell, J.S., et al., *Exploring DeltaR(2) * and DeltaR(1) as imaging biomarkers of tumor oxygenation.* J Magn Reson Imaging, 2013. **4**(10): p. 23987.
30. Newbold, K., et al., *An exploratory study into the role of dynamic contrast-enhanced magnetic resonance imaging or perfusion computed tomography for detection of intratumoral hypoxia in head-and-neck cancer.* Int J Radiat Oncol Biol Phys, 2009. **74**(1): p. 29-37.
31. Jackson, A.S., et al., *Dynamic contrast-enhanced MRI for prostate cancer localization.* Br J Radiol, 2009. **82**(974): p. 148-56.
32. Evelhoch, J.L., *Key factors in the acquisition of contrast kinetic data for oncology.* J Magn Reson Imaging, 1999. **10**(3): p. 254-9.
33. Tofts, P.S., et al., *Estimating kinetic parameters from dynamic contrast-enhanced T(1)-weighted MRI of a diffusable tracer: standardized quantities and symbols.* J Magn Reson Imaging, 1999. **10**(3): p. 223-32.
34. Turkbey, B., et al., *The role of dynamic contrast-enhanced MRI in cancer diagnosis and treatment.* Diagn Interv Radiol, 2010. **16**(3): p. 186-92.
35. Yankeelov, T.E., et al., *Quantitative pharmacokinetic analysis of DCE-MRI data without an arterial input function: a reference region model.* Magn Reson Imaging, 2005. **23**(4): p. 519-29.
36. Hicks, R.J., *Beyond FDG: novel PET tracers for cancer imaging.* Cancer Imaging, 2003. **4**(1): p. 22-4.
37. Hendrickson, K., et al., *Hypoxia imaging with [F-18] FMISO-PET in head and neck cancer: Potential for guiding intensity modulated radiation therapy in overcoming hypoxia-induced treatment resistance.* Radiotherapy and Oncology, 2011. **101**(3): p. 369-375.

38. Dukart, J., et al., *Combined evaluation of FDG-PET and MRI improves detection and differentiation of dementia.* PLoS ONE, 2011. **6**(3): p. 0018111.
39. Szeto, M.D., et al., *Quantitative metrics of net proliferation and invasion link biological aggressiveness assessed by MRI with hypoxia assessed by FMISO-PET in newly diagnosed glioblastomas.* Cancer Res, 2009. **69**(10): p. 4502-9.
40. Hendrickson, K., et al., *Hypoxia imaging with [F-18] FMISO-PET in head and neck cancer: potential for guiding intensity modulated radiation therapy in overcoming hypoxia-induced treatment resistance.* Radiother Oncol, 2011. **101**(3): p. 369-75.
41. Toma-Dasu, I., et al., *Dose prescription and treatment planning based on FMISO-PET hypoxia.* Acta Oncol, 2012. **51**(2): p. 222-30.
42. Tatum, J.L., et al., *Hypoxia: importance in tumor biology, noninvasive measurement by imaging, and value of its measurement in the management of cancer therapy.* Int J Radiat Biol, 2006. **82**(10): p. 699-757.
43. Taylor, N.J., et al., *BOLD MRI of human tumor oxygenation during carbogen breathing.* J Magn Reson Imaging, 2001. **14**(2): p. 156-63.
44. Krohn, K.A., J.M. Link, and R.P. Mason, *Molecular imaging of hypoxia.* J Nucl Med, 2008. **49**(2): p. 045914.
45. Muller, A., et al., *Intracranial tumor response to respiratory challenges at 3.0 T: impact of different methods to quantify changes in the MR relaxation rate R2*.* J Magn Reson Imaging, 2010. **32**(1): p. 17-23.
46. Rakow-Penner, R., B. Daniel, and G.H. Glover, *Detecting blood oxygen level-dependent (BOLD) contrast in the breast.* J Magn Reson Imaging, 2010. **32**(1): p. 120-9.
47. Baudelet, C. and B. Gallez, *How does blood oxygen level-dependent (BOLD) contrast correlate with oxygen partial pressure (pO2) inside tumors?* Magn Reson Med, 2002. **48**(6): p. 980-6.
48. Dunn, J.F., et al., *Changes in oxygenation of intracranial tumors with carbogen: a BOLD MRI and EPR oximetry study.* J Magn Reson Imaging, 2002. **16**(5): p. 511-21.
49. Elas, M., et al., *Quantitative tumor oxymetric images from 4D electron paramagnetic resonance imaging (EPRI): methodology and comparison with blood oxygen level-dependent (BOLD) MRI.* Magn Reson Med, 2003. **49**(4): p. 682-91.
50. Peschke, P., et al., *Differential sensitivity of three sublines of the rat Dunning prostate tumor system R3327 to radiation and/or local tumor hyperthermia.* Radiat Res, 1998. **150**(4): p. 423-30.
51. Isaacs, J.T., et al., *Genetic instability coupled to clonal selection as a mechanism for tumor progression in the Dunning R-3327 rat prostatic adenocarcinoma system.* Cancer Res, 1982. **42**(6): p. 2353-71.
52. Zimny, M., et al., *FDG--a marker of tumour hypoxia? A comparison with [18F]fluoromisonidazole and pO2-polarography in metastatic head and neck cancer.* Eur J Nucl Med Mol Imaging, 2006. **33**(12): p. 1426-31.
53. Piert, M., et al., *Introducing fluorine-18 fluoromisonidazole positron emission tomography for the localisation and quantification of pig liver hypoxia.* Eur J Nucl Med, 1999. **26**(2): p. 95-109.
54. Gagel, B., et al., *pO2 Polarography Versus Positron Emission Tomography ([18F] Fluoromisonidazole, [18F]-2-Fluoro-2-Deoxyglucose): An Appraisal of Radiotherapeutically Relevant Hypoxia.* Strahlentherapie und Onkologie, 2004. **180**(10): p. 616-622.

55. Riss, P.J., et al., *Synthesis of [18F]Fluoromisonidazole (1-(2-Hydroxy-3-[18F]Fluoropropyl)-2-Nitroimidazole, [18F]FMISO)*, in *Radiochemical Syntheses*2012, John Wiley & Sons, Inc. p. 41-49.
56. Alonzi, R., et al., *Carbogen breathing increases prostate cancer oxygenation: a translational MRI study in murine xenografts and humans.* Br J Cancer, 2009. **100**(4): p. 644-8.
57. Rijpkema, M., et al., *Effects of breathing a hyperoxic hypercapnic gas mixture on blood oxygenation and vascularity of head-and-neck tumors as measured by magnetic resonance imaging.* Int J Radiat Oncol Biol Phys, 2002. **53**(5): p. 1185-91.
58. O'Connor, J.P., et al., *Preliminary study of oxygen-enhanced longitudinal relaxation in MRI: a potential novel biomarker of oxygenation changes in solid tumors.* Int J Radiat Oncol Biol Phys, 2009. **75**(4): p. 1209-15.
59. Matsumoto, K., et al., *MR assessment of changes of tumor in response to hyperbaric oxygen treatment.* Magn Reson Med, 2006. **56**(2): p. 240-6.
60. Young, I.R., et al., *Enhancement of relaxation rate with paramagnetic contrast agents in NMR imaging.* J Comput Tomogr, 1981. **5**(6): p. 543-7.
61. Mason, R.P., et al., *Non-invasive determination of tumor oxygen tension and local variation with growth.* Int J Radiat Oncol Biol Phys, 1994. **29**(1): p. 95-103.
62. Mason, R.P., et al., *Regional tumor oxygenation and measurement of dynamic changes.* Radiat Res, 1999. **152**(3): p. 239-49.
63. Zhao, D., et al., *Differential oxygen dynamics in two diverse Dunning prostate R3327 rat tumor sublines (MAT-Lu and HI) with respect to growth and respiratory challenge.* Int J Radiat Oncol Biol Phys, 2002. **53**(3): p. 744-56.
64. Zhao, D., et al., *Tumor oxygen dynamics: correlation of in vivo MRI with histological findings.* Neoplasia, 2003. **5**(4): p. 308-18.
65. Zhao, D., et al., *Tumor oxygen dynamics with respect to growth and respiratory challenge: investigation of the Dunning prostate R3327-HI tumor.* Radiat Res, 2001. **156**(5 Pt 1): p. 510-20.
66. Christen, T., et al., *Is T2* enough to assess oxygenation? Quantitative blood oxygen level-dependent analysis in brain tumor.* Radiology, 2012. **262**(2): p. 495-502.
67. Yao, X., et al., *A novel orthotopic tumor model to study growth factors and oncogenes in hepatocarcinogenesis.* Clin Cancer Res, 2003. **9**(7): p. 2719-26.
68. Wang, Y., et al., *An orthotopic metastatic prostate cancer model in SCID mice via grafting of a transplantable human prostate tumor line.* Lab Invest, 2005. **85**(11): p. 1392-404.
69. Somers, K.D., et al., *Orthotopic treatment model of prostate cancer and metastasis in the immunocompetent mouse: efficacy of flt3 ligand immunotherapy.* Int J Cancer, 2003. **107**(5): p. 773-80.
70. Lelekakis, M., et al., *A novel orthotopic model of breast cancer metastasis to bone.* Clin Exp Metastasis, 1999. **17**(2): p. 163-70.
71. Chen, X., et al., *An orthotopic model of lung cancer to analyze primary and metastatic NSCLC growth in integrin alpha1-null mice.* Clin Exp Metastasis, 2005. **22**(2): p. 185-93.
72. Killion, J., R. Radinsky, and I. Fidler, *Orthotopic Models are Necessary to Predict Therapy of Transplantable Tumors in Mice.* Cancer and Metastasis Reviews, 1998. **17**(3): p. 279-284.

73. Gaustad, J.V., et al., *Intratumor heterogeneity in blood perfusion in orthotopic human melanoma xenografts assessed by dynamic contrast-enhanced magnetic resonance imaging.* J Magn Reson Imaging, 2005. **21**(6): p. 792-800.
74. Kim, H., et al., *Early therapy evaluation of combined cetuximab and irinotecan in orthotopic pancreatic tumor xenografts by dynamic contrast-enhanced magnetic resonance imaging.* Mol Imaging, 2011. **10**(3): p. 153-67.

BIOGRAPHICAL INFORMATION

Rashmi Reddy Pabhathi Reddy was born in Hyderabad, India also known as the city of pearls in the year 1990. She was good at cultural activities and leadership skills. Her skills helped her to get a job in Tata Consultancies Limited and InfoTech, India, as a software engineer, but her enthusiasm to pursue higher education, motivated her to join Masters Degree in Bioengineering at University of Texas at Arlington, 2011. She has many IEEE and national publications from undergraduate studies in India. Her research interests include tumor hypoxia, electronics and instrumentations. She is looking for a job opportunity to further enhance her skills and abilities and apply her past work experience.